



UNIVERSITÀ DEGLI STUDI DELL'AQUILA
DIPARTIMENTO DI SCIENZE CLINICHE APPLICATE E BIOTECNOLOGIE

Dottorato di Ricerca in Medicina Sperimentale

Curriculum Biotecnologie e scienze biochimiche

XXXVI ciclo

Titolo della tesi

**Identification of new molecules involved in
osteoblast homeostasis**

SSD: Bio/17 - ISTOLOGIA

Dottoranda

Chiara Puri

Chiara Puri

Coordinatore del corso

Prof. ssa Mariagrazia Perilli

Mariagrazia Perilli

Tutor

Prof. ssa Nadia Rucci

Nadia Rucci

a.a. 2022/2023

Table of Contents

Summary	4
Chapter 1: “Introduction”	6
1. Introduction	7
1.1 The bone tissue.....	7
1.2 Anatomy and macroscopic organization.....	7
1.3 The bone matrix	9
1.4 Bone cells.....	10
1.5 Bone remodeling	16
2. Osteoporosis and disuse osteoporosis	18
2.1 Definition	18
2.2 Disuse osteoporosis in long-term bed rest and paralysis	19
2.3 Disuse osteoporosis in space flight	20
2.4 How to model simulated microgravity.....	21
3. Aim of the work	26
Chapter 2: “Pre-proenkephalin 1 is downregulated under unloading and is involved in osteoblast biology”.....	28
1. Abstract	29
2. Introduction.....	29
3. Materials and methods	31
3.1 Materials.....	31
3.2 Animals	31
3.3 Hindlimb suspension and in vivo treatment with botulin toxin A	32
3.4 Head Down tilt Bed Rest (HDBR) experiment.....	32

3.5	Osteoblast primary cultures	32
3.6	Comparative real-time RT-PCR.....	33
3.7.	MicroCT analysis.....	33
3.8	Bone histomorphometry.....	34
3.9	Bone turnover biomarkers.....	34
3.10	Statistics	34
4.	Results.....	35
4.1	Mechanical unloading induces <i>Penk1</i> downregulation in mouse and human	35
4.2	Lack of an overt bone phenotype in <i>Penk1</i> KO mice.	36
4.3	<i>Penk1</i> regulates osteoblast differentiation and activity.....	40
5.	Discussion	43
Chapter 3: “Effect of Lipocalin-2 ablation on osteoblasts subjected to mechanical unloading.”....		46
1.	Abstract	47
2.	Introduction	47
3.	Materials and methods	48
3.1	Materials.....	48
3.2	Animals	49
3.3	Osteoblast primary cultures	49
3.4	Comparative real-time RT-PCR.....	50
3.5	ELISA assay.....	50
3.6	Hindlimb suspension.....	50
3.7	MicroCT analysis.....	51
3.8	Bone histomorphometry.....	51
3.9	Statistics	52
4.	Results.....	52
4.1	Effect of <i>Lcn2</i> ablation on osteoblasts subjected to simulated microgravity	52

4.2	Effect of Lcn2 ablation in the bones of mice subjected to mechanical unloading.....	56
5.	Discussion	59
Chapter 4:	“General discussion and conclusions”	61
1.	General discussion and conclusions.....	62
Chapter 5:	“References”	65
	References.....	66
Chapter 6:	“Achievements”	79
	Curriculum Vitae et Studiorum.....	80

Summary

Osteoblasts are bone forming cells that work in cooperation with osteoclasts, which resorb bone, in a continuous cycle of bone remodeling. Since bone remodeling is crucial for preserving skeletal integrity and functionality, events, such as mechanical unloading, perturb this equilibrium, leading to pathological conditions, like disuse osteoporosis.

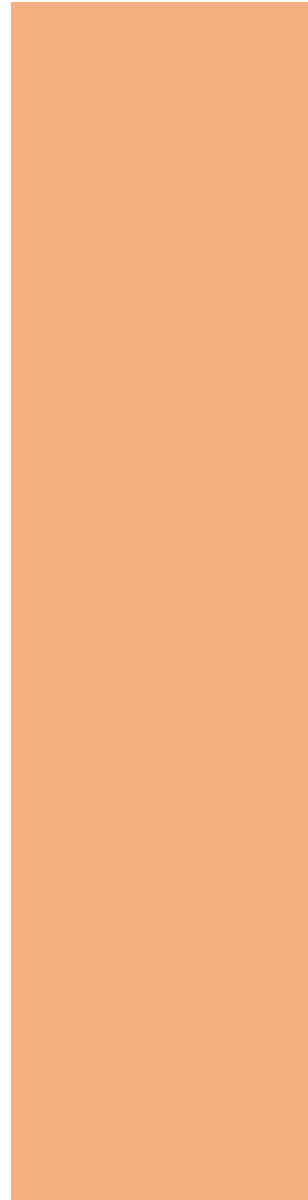
In a previous work conducted in our laboratory, Lipocalin 2 (*LCN2*) and Pre-proenkephalin 1 (*PENK1*) were identified as the most up- and down-regulated genes in osteoblasts subjected to mechanical unloading.

Starting from this data, during my PhD I focused my research to evaluate the involvement of these molecules in osteoblasts homeostasis, in particular in response to mechanical unloading.

In Chapter 2 we confirmed *PENK1* downregulation due to mechanical unloading in both human and animal models of mechanical unloading. We also observed high expression of *Penk1* in mouse in mouse femurs and calvariae cleaned from bone marrow, and this expression progressively increased during osteoblast differentiation. Surprisingly, *Penk1* knock out (*Penk1*^{-/-}) mice did not show bone phenotype compared to the WT littermates; however silenced *Penk 1* in mature osteoblasts we observed an impairment of the Wnt pathway, while primary osteoblasts isolated from *Penk1*^{-/-} mouse calvariae showed an impairment of their metabolic and Alp activities, along with a lower nodule mineralization ability, compared to cells isolated from WT mice. Moreover, in a CFU-Fibroblastic assay, using bone marrow cells isolated from tibias, we observed a decrease of ability to form Alp-positive colonies in *Penk1*^{-/-} versus WT mice, suggesting a cell autonomous positive effect of *Penk1* in osteoblasts. In line with this, treatment of osteoblasts with Met-enkephalin, *Penk1* encoded peptide, increased *Osx* and *Colla1* mRNAs, and enhanced nodule mineralization.

In the second part of this work (Chapter3) we investigated whether genetic ablation of this gene can counteract the inhibitory effect of microgravity on osteoblast differentiation. Our results demonstrated that, at least *in vitro*, *Lcn2* genetic ablation counteracts the reduction of *Runx2* and *Osx* transcriptional expression induced by microgravity. Moreover, *Lcn2* ablation also prevents the increase of RANKL/OPG ratio observed in the conditioned media of WT osteoblasts cultured under unloading conditions. However, in the mice subjected to mechanical unloading, the lack of *Lcn2* is not sufficient to counteract the bone loss due to mechanical unloading and disuse, although it is enough to prevent the number and the surface area of osteoblasts from decreasing, as compared to WT littermates.

In conclusion, although future studies will be required to fully understand the mechanism of bone detrimental adaptation after mechanical unloading, the work reported in this dissertation adds another piece of knowledge, demonstrating the role that *Penk1* and *Lcn2* play in this event, as well as the contribution of *Penk1* in osteoblast homeostasis. It is also important to point out that these studies are exploitable and applicable to those pathological circumstances in which patients experience disuse induced-bone loss due to of paralysis or neuromuscular disorders, as well as in case of long-duration space flights.



Chapter 1: “Introduction”

1. Introduction

1.1 The bone tissue

The bone tissue exerts many important functions, including locomotion, protection of soft organs, metabolic reserve of calcium and phosphate, and harbouring of bone marrow¹. Unlike its marble-like appearance, bone is far from immutable being an extremely dynamic and metabolically-active tissue, that is renewed throughout our entire lifetimes⁷⁵ Like other connective tissues, bone has an abundant organic extracellular matrix (ECM) mainly composed of collagen fibers (predominantly type I), glycoproteins and proteoglycans. What sets bone apart from the other connective tissues is its inorganic matrix component composed of mainly hydroxyapatite (a form of calcium phosphate), along with low amounts of calcium carbonate, magnesium hydroxide, fluoride and sulphate. During growth, bone has to change shape and size to accommodate the growing organism, in a process called bone modeling, while after puberty and final height is reached, it undergoes a continuous remodeling process through which old bone is replaced by a new one, in order to preserve its mechanical properties^{2,3}. The remodeling process requires the three main cell types present in the bone tissue to work in concert: (i) osteoblasts, the bone forming cells, (ii) osteoclasts, the bone resorption cells, and (iii) osteocytes, mechanosensors and controllers of bone remodeling^{1,5}.

1.2 Anatomy and macroscopic organization

Bone can be classified according to its morphology and structure, from a macroscopic to a nanoscopic level⁵. Macroscopically, the 206 bones that form the human skeleton can be divided into five types: long, short, flat, irregular and sesamoid⁴. Long bones, such as the femur and tibia, consist of a cylindrical-like body whose length is greater than its width, called diaphysis, which ends in two epiphyses, as well as a transition zone between them, the metaphysis⁴. The diaphysis is a hollow cylinder in which the medullary cavity is housed and whose wall consists of dense, compact bone tissue, known as cortical bone. Proceeding from the diaphysis to the epiphysis, the bone tissue thins out and the free space is occupied by trabecular bone^{4,5}. The trabeculae are thin calcified structures that form a network, the cavities thus formed are continuous with the diaphyseal medullary cavity and are occupied by bone marrow⁵. Short bones, such as the carpus, tarsus, and vertebrae, are characterized by similar length and diameter; while flat bones have a large surface area and are thin in cross section. Examples of irregular bones are

vertebrae, difficult to describe in terms of shape. Finally, the sesamoid bones, like the patella, are small round-shaped bones with the main function of protecting the tendons from compression ^{1,5}.

From a structural point of view, human bone can be classified into woven and lamellar bone ⁴. The former is only found in embryonic and neonatal bones and during fracture healing and is characterized by collagen fibers organized in randomly oriented bundles, resulting in a weaker but more flexible bone compared to lamellar bone (**Figure 1a**). In contrast, in lamellar bone the matrix is organized in microscopically thin layered sheets known as lamellae, in which collagen fibers are arranged in parallel oriented bundles whose orientation varies between adjacent lamellae (**Figure 1b**) ^{1,5}.

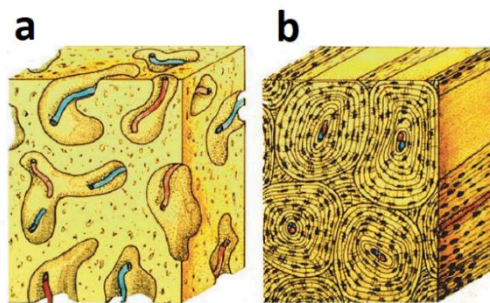


Figure 1: Woven and lamellar bone. Diagram illustrating the difference between (a) woven and (b) lamellar bone. Woven bone, due to the random organization of collagen fibres, displays a disorganised appearance, while in lamellar bone the matrix is organized in microscopically thin layered sheets known as lamellae in which collagen fibers are arranged in parallel oriented manner (Source: adapted from: Bone Structure, Development and Bone Biology: Bone Pathology - Scientific Figure on ResearchGate. Available from: https://www.researchgate.net/figure/Diagram-of-immature-and-mature-bone-Immature-woven-bone-displays-a-disorganized_fig2_224929158).

In trabecular bone and periosteum, which is an envelope of connective tissue that lines external bone surfaces, the lamellae are arranged parallel to each other and lodged along a flat surface, while in cortical bone they are deposited around a central canal, known as Haversian canal. In fact, cortical bone is organized in the Haversian systems or osteons (**Figure 2**). In the center of each osteon there is the Haversian canal, which is coated by endosteum, a layer of connective tissue that lines the inner surfaces of bones and contains blood vessels and nerves. In addition to Haversian canal, Volkmann's canals ensure communication between adjacent osteons by also connecting Haversian blood vessels. The appearance of an osteon is that of a cylinder running parallel to the long axis of the diaphysis. In the interstices between the osteons there are irregular areas of lamellar bone, which are residues of previous remodeled osteons. In the outermost and innermost layers of cortical bone, called the outer and inner circumferential

lamellae respectively, there are no Haversian canals and the lamellae run parallel with periosteal and endosteal surfaces.^{1,5}

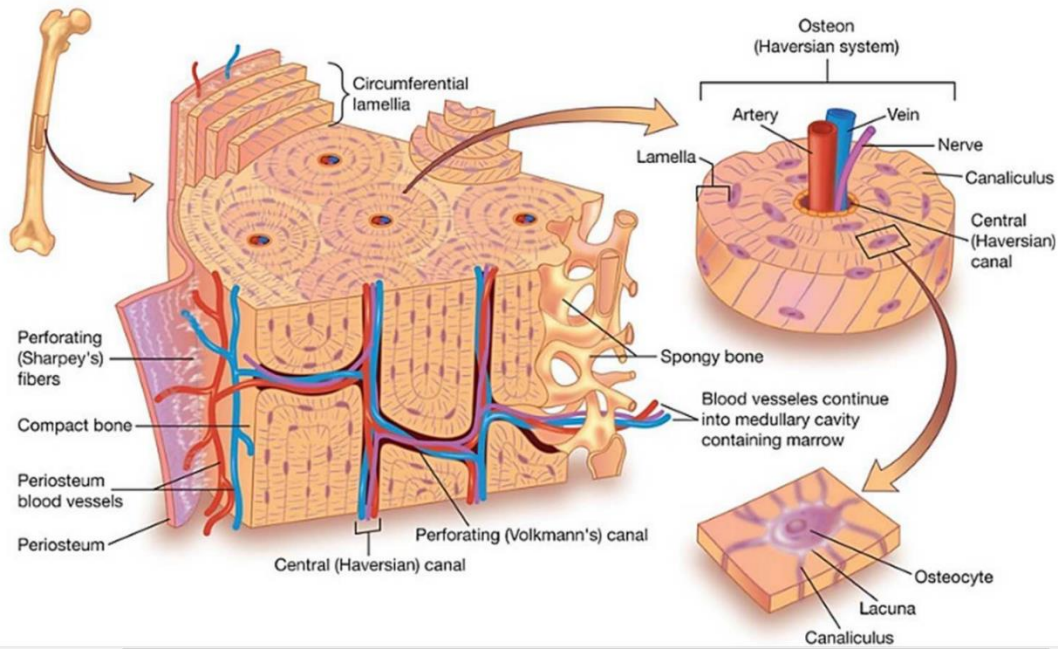


Figure 2: Microscopic structure of bone. Schematic representation of the Haversian system and of lamellar bone (Source: adapted from <https://www.vectorstock.com>.)

1.3 The bone matrix

The bone extracellular matrix is quite unique, since it is mineralized and therefore composed of both inorganic and organic components³. The mineral component of the matrix provides to the bone tissue the mechanical rigidity and load-bearing strength, while the organic component is responsible for its flexibility and elasticity. About 90% of the mineral component consists of hydroxyapatite crystals, while the main constituent of the organic matrix, which accounts for 35% of the dry weight of all the tissue, consists of collagen type I fibers oriented parallel to each other and arranged in layers that form the typical lamellar structure of the bone⁶. This organization gives reason for the extensive resistance and stiffness of the bone. Non collagenous proteins in the organic matrix, such as osteonectin, osteocalcin, osteopontin, proteoglycans, cytokines and growth factors, are involved in many functions, including a structural function but also regulation of bone mineral deposition and turnover, and regulation of bone cells activity^{6,7}.

1.4 Bone cells

1.4.1 Osteoblasts

Osteoblasts are cuboidal-shaped cells (**Figure 3**) accounting for the 4–6% of the total resident bone cells. Osteoblasts are in charge for depositing and calcifying the bone matrix¹. Osteoblasts can be observed lining the bone matrix in often long lines of cells (>3), which are in contact with the neighboring ones through *adherent* and gap junctions^{8,9}. The latter not only provide adhesion but also intercellular communication⁸.

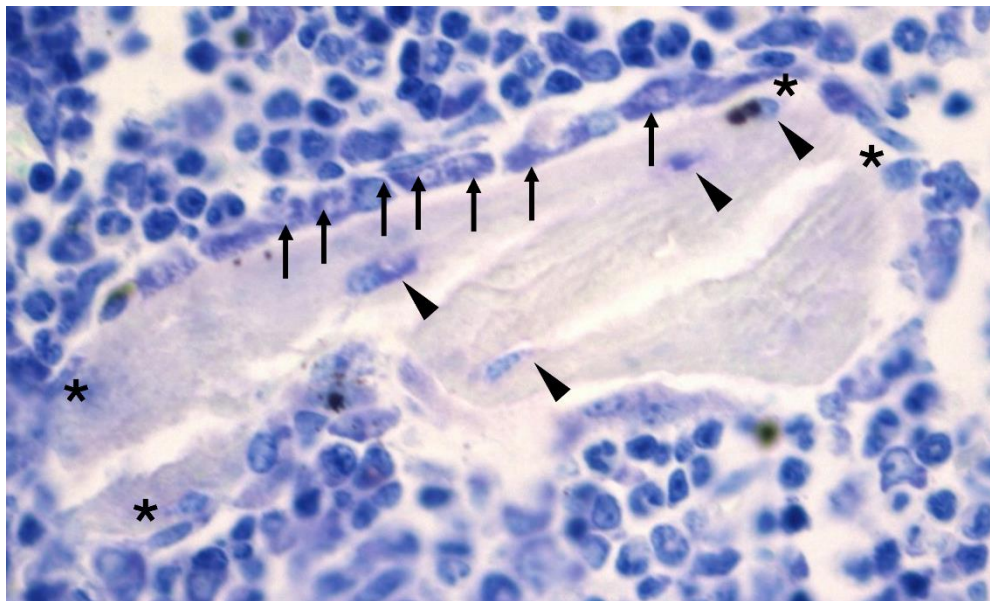


Figure 3: Osteoblasts, osteocytes, and bone-lining cells morphology. Toluidine blue staining of a mouse tibia showing osteoblasts (arrows), osteocytes (arrowhead) and bone-lining cells (asterisks) (male, 8 weeks of age, original magnification 400×).

Like other cells of connective tissues such as adipocytes, chondrocytes, fibroblasts and myoblasts, osteoblasts arise from mesenchymal stem cells (MSCs)⁹. The commitment of MSCs to an osteo/chondroprogenitor line is regulated by specific molecules, such as those belonging to the Wingless-related integration site (WNT) and Bone Morphogenetic Proteins (BMPs)²⁸ family (**Figure 4**). A very important role is played by WNT proteins by means of both the canonical and non-canonical WNT signaling pathways. The canonical WNT pathway is initiated by the binding of WNT ligand to Frizzled (FZD) receptor and to Low-density lipoprotein Receptor-related Proteins 5/6 (LRP-5/6) coreceptor, expressed on osteoprogenitor cell plasma membrane²⁹. This binding promotes an intracellular signaling

cascade which involves a multi-protein complex, including Glycogen Synthase Kinase 3 β (GSK3 β), Axin, Adenomatous Polyposis Coli (APC) and Dishevelled (DSH) proteins. The assembled complex inhibits the GSK3 β -mediated β -catenin phosphorylation and its ubiquitin-mediated degradation, leading to β -Catenin stabilization and translocation into the nucleus. Once in the nucleus, β -Catenin interacts with T cell-specific transcription factor/Lymphoid Enhancer-binding Factor (TCF/LEF) and promotes the transcription of the master regulators of osteoblast differentiation Runt-related transcription factor 2 (*RUNX2*) and Osterix (*OSX*), among other important osteoblast differentiation genes³⁰. Genetic evidence that β -Catenin is required for osteoblast development has been demonstrated by Hu and colleagues in 2005⁷³, while Tu X *et al*⁶⁴ proved that *WNT-GAQ/11 -PKCd* non-canonical pathway operates in mammalian osteoprogenitors in order to promote osteoblast development. Another novel noncanonical signaling pathway enhancing osteogenic differentiation of MSCs is reported by Chang J *et al*⁶⁵, according to which *WNT-4* plays a critical role in osteoprogenitor development.

Going through the differentiation pathway, pre-osteoblasts express *AKP2*, the gene coding for Alkaline phosphatase (ALP), which is considered one of the early markers of osteoblast differentiation along with Collagen 1A1 (*COL1a1*, which is kept very active throughout the differentiation process) and Osterix. Mature osteoblasts also express receptors for parathyroid hormone (PTH), estrogens (ERs), vitamin D3 (VDR), and produce bone matrix proteins, such as bone sialoproteins and osteocalcin¹⁻⁹⁻¹⁰. When observed by transmission electron microscopy, mature osteoblasts have a very abundant endoplasmic reticulum and an extensively developed Golgi apparatus, their cytoplasm is rich in ribosomes and secretory vesicles, and the nucleus is euchromatic, with large, well-defined nucleoli^{11,12}. In fact, the main activity of osteoblasts is the production and secretion of the organic component of the ECM, as well as the deposition of its mineral component, which is consistent with their appearance and organelle composition⁹.

Osteoblasts also produce several cytokines involved in the regulation of osteoclasts, such as Macrophages-Colony Stimulating Factor (M-CSF), responsible for the survival and growth of pre-osteoclasts, Receptor Activator of Nuclear Factor- κ B Ligand (RANKL), which is crucial for osteoclast differentiation, and osteoprotegerin (OPG), a RANKL decoy receptor that prevents RANKL from binding to RANK and therefore also osteoclastogenesis¹⁰⁻¹³. In addition, recent papers highlight unexpected osteogenic functions of RANKL. In particular, it has been identified the existence of an autocrine loop possibly activated by the secreted cytokine in MSCs. *RANKL*^{-/-} MSCs, in fact, show a reduction in osteogenic capacity and, in parallel, restoration of RANKL production ameliorates the defect in the osteoblast lineage⁶⁶. Moreover, osteoclast derived vesicular RANK is able to promote bone

formation by binding to osteoblast RANKL. This interaction activates RANKL reverse signaling, which in turns activates RUNX2⁶⁷.

Osteoblast is however only a phase in the osteoblast-lineage cell, which once completed its work as bone matrix builder, can go to three different fates: apoptosis, become an osteocyte (see below), or giving rise to bone lining cells, which are flat and quiescent cells covering the resting bone surfaces until a stimulus reactivates them⁹⁻¹³.

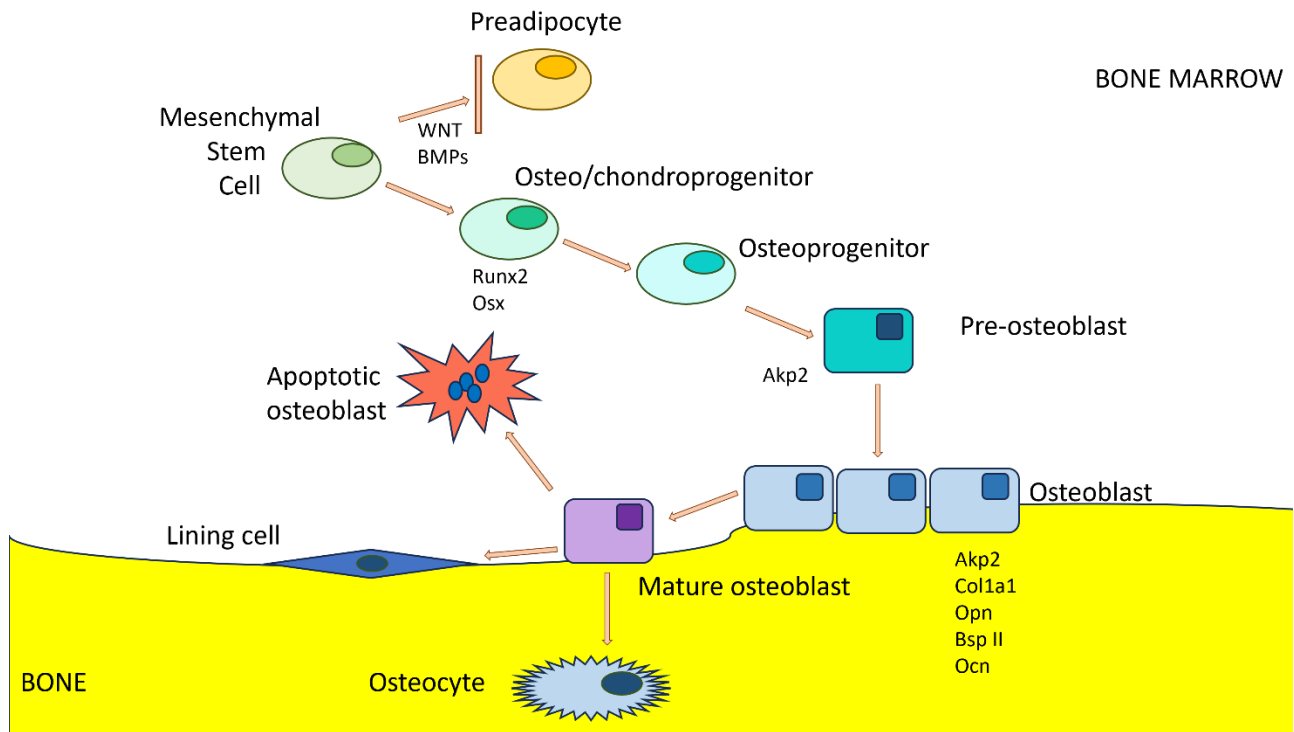


Figure 4: Schematic representation of the osteoblast differentiation process. Osteoblasts derive from mesenchymal stem cells and their differentiation is promoted by Wingless (WNT) and bone morphogenic protein (BMP) pathways. The activation of these pathways promotes *RUNX2* and *OSX* expression in osteo-chondroprogenitors, leading to their differentiation towards osteoprogenitors and then pre-osteoblasts, which express *ALP*, one of the earliest markers of osteoblast differentiation. Later on osteoblasts will express other specific markers, such as *COL1A1*, *OPN*, *BSP II* and *OCN*. Mature osteoblasts ultimately will be embedded in the bone matrix as terminally differentiated osteocytes, or will become a bone lining cell, or will die by apoptosis.

1.4.2 *Osteocytes*

The evolution from osteoblasts to osteocytes is characterized by a drastic change in cell shape. In fact, from a polygonal morphology that characterizes mature osteoblasts, the cells become flattened and with several polarized cytoplasmic protrusions, some of which extend towards the mineralization front, while others extend towards the vascular space or towards other osteocytes, forming the so-called lacunar-canalicular system (LCS) ⁹. In the last decades, some specific markers for osteocytes differentiation have been identified, including phosphate regulating neutral endopeptidase on the chromosome X (PHEX), dentin matrix protein 1 (DMP1), and E11/gp38 for early osteocytes; while RANKL, sclerostin (SOST), fibroblast growth factor 23 (FGF23), and matrix extracellular phosphoglycoprotein (MEPE) are mainly expressed by mature osteocytes ¹⁴. Although osteocytes are the most abundant cell population in bone tissue (about 90-95% of the total bone cells), for a long time they were considered quiescent cells derived from osteoblasts trapped in the bone mineralized matrix. Currently, thanks to new technologies and improved isolation protocols, additional functions have been attributed to osteocytes ¹. Indeed, osteocytes are very long-lived cells, having an estimated life span up to 25 years, during which they play a role as mechano-sensors, as well as in the local activation of bone turnover and in the release of FGF23, a hormone that regulates tubular phosphate reabsorption by the kidney ¹¹. Another molecule produced by osteocytes playing a crucial role in the regulation of bone formation is SOST, a glycoprotein that inhibits proliferation and differentiation of osteoblasts by binding to LRP5/6 and thus blocking the Wnt/ β -catenin signaling pathway ³⁶. For this reason, antibodies against sclerostin are successfully used in osteoporosis treatment ³⁵.

Since osteocytes are fully surrounded by LCS, these cells can sense shear stress from mechanical stimulation, convert mechanical signals into internal biochemical signals, and eventually transduce these into different biological functions, playing an important role in bone remodeling regulation ³⁷. Indeed, osteocytes regulate both bone formation by osteoblasts and bone resorption by osteoclasts, via both cell-cell interactions, and also through the release of soluble mediators ³⁸. Indeed osteocytes are a source of OPG and RANKL, and the regulation of their production provides a mechanism by which osteocytes can regulate osteoclast-mediated bone resorption ³⁹. Moreover, mice in which RANKL expression was selectively suppressed in osteocytes showed an osteopetrotic phenotype, resistant to bone loss induced by mechanical unloading after tail suspension. Osteocytes also secrete other molecules with the ability to modulate bone remodeling, including small mediators like prostanoids, nitric oxide, and nucleotides, as well as a huge variety of cytokines and growth factors, such as insulin-like growth factor-1 (IGF-1), vascular endothelial cell growth factor (VEGF) and Transforming Growth Factor- β (TGF- β).

In addition, PTH increases RANKL osteocytes production, therefore osteocytes are mediators of the PTH effect on bone resorption ³⁹.

1.4.3 Osteoclasts

Osteoclasts are giant multinucleated cells belonging to the monocyte-macrophage lineage, originating from the fusion of mononuclear precursors. Osteoclasts contain 4 to 50 well defined nuclei each, and their main job is resorbing bone ⁹⁻¹⁵. They are located in the so-called Howship's lacunae, depressions of the bone surface originating from matrix resorption by the osteoclasts themselves ¹⁵. Osteoclasts are polarized cells showing different plasma membrane domains: the apical membrane, characterized by the “sealing zone”, a bone-facing area with specialized adhesion structures called podosomes; the “ruffled border”, a system of membrane expansions that increase the membrane surface between osteoclasts and the bone matrix, facilitating the resorption process; the basolateral membrane, rich in ion channels and presenting a secretory domain essential for releasing the digested matrix components into the bloodstream ¹⁷.

The cytoplasm is rich in vacuoles, with numerous mitochondria, lysosomes, and multiple Golgi apparati ¹⁶ (**Figure 5**).

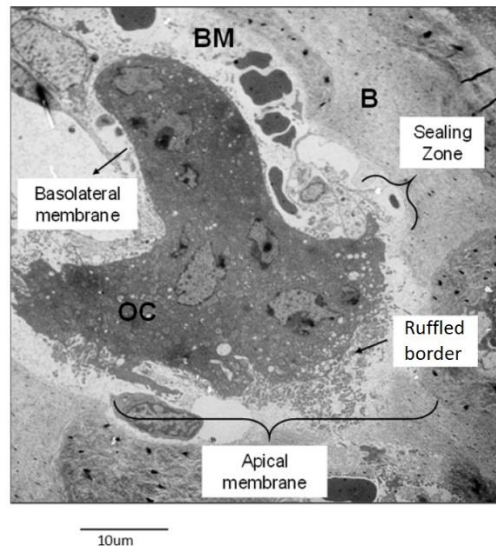


Figure 5: Osteoclasts morphology. Transmission electron microscopy (TEM) picture of an osteoclast from an Epon-embedded tibia from a C57/B6 mouse. Scale 10 μ m. B: bone. OC: osteoclast. BM: bone marrow. (Source: Maurizi A, Rucci N. 2018 ¹⁷)

As already described, osteoclast differentiation is regulated by specific cytokines, such as M-CSF and RANKL; the first stage involves the commitment of hematopoietic stem cells (HSCs) to the macrophage lineage; this is followed by the acquisition of positivity for the tartrate-resistant acid phosphatase (TRAcP) enzyme and for calcitonin receptor, thus giving rise to an osteoclast precursor and, finally, the fusion of the precursors into mature polynucleated osteoclasts ¹⁷. M-CSF binds to the c-Fms receptor located on the preosteoclast surface, thus inducing trans-phosphorylation of tyrosine residues in the receptor's cytoplasmic tail, which in turn activates a downstream pathway that promotes the proliferation and survival of osteoclast precursors. Moreover, the RANKL-RANK interaction on the surface of osteoclast precursors results in the recruitment of proteins of the TNF receptor-associated factor (TRAF) family, followed by the nuclear translocation of the nuclear factor κ -activated B-cell light-chain-enhancer (NF κ B) and nuclear factor of activated T-cell nuclear factor 1 (NFATc1). These transcription factors promote the expression of osteoclast specific genes, such as TRAcP, Cathepsin K, Osteoclast Associated Receptor (OSCAR), Dendritic Cell-Specific Transmembrane Protein (DC-STAMP) and Matrix Metalloproteinase (MMP)-9 and -14, ^{18, 19} (**Figure 6**).

Tumour Necrosis Factor- α (TNF- α), Interleukin (IL-) 1 β and 6 and other inflammatory molecules can also support osteoclastogenesis through activation of the NF κ B pathway ²⁰.

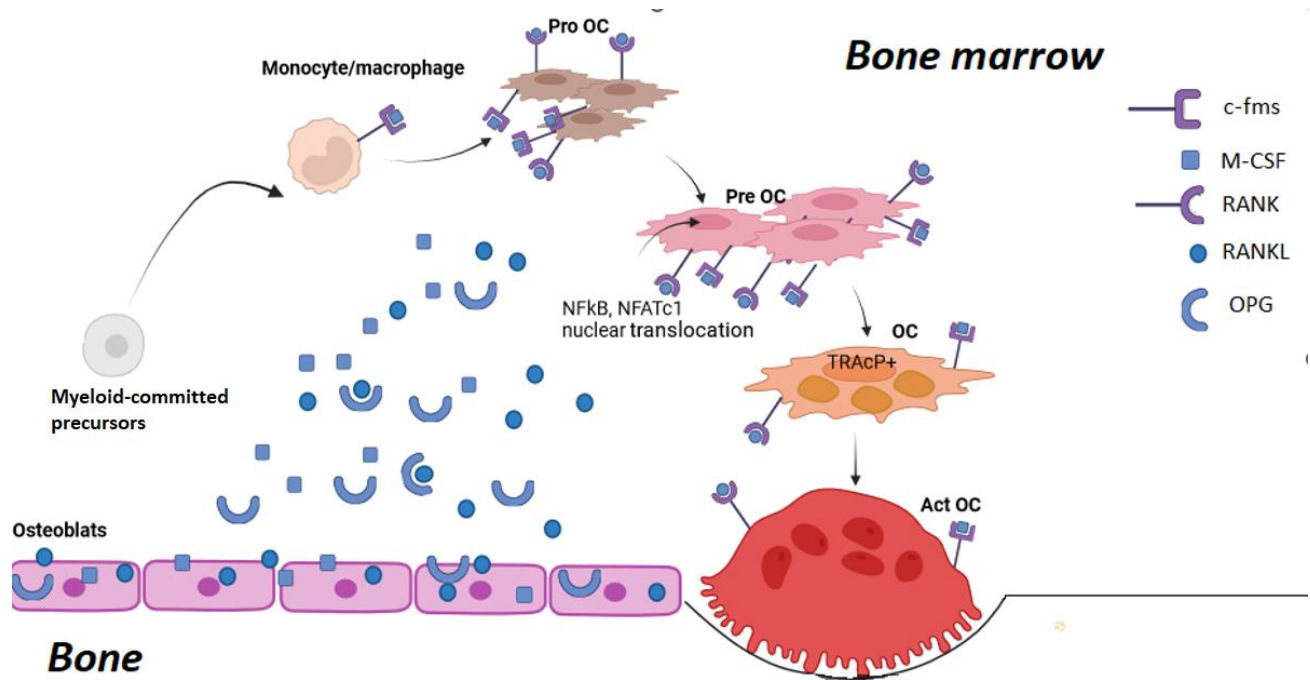


Figure 6: Osteoclast differentiation. Osteoclasts arise from myeloid-committed precursors that are able to differentiate into monocytes/macrophages or dendritic cells. Monocytes/macrophages then differentiate into osteoclast progenitors (Pro OC), pre-osteoclasts (Pre OC), osteoclasts (OC) and then active OC (Act OC). (Source: created in BioRender.com).

1.5 Bone remodeling

Bone remodeling was first defined by Frost²¹ as a cycle by which bone tissue integrity and functionality is preserved, consisting of a series of well-programmed cellular events that lead to the resorption of old and damaged bone tissue and the deposition of new bone, without however leading to changes in the shape of the bone itself^{8, 21, 22}. This process takes place in the Bone Multicellular Units (BMU), where osteoblasts and osteoclasts closely collaborate, and can be divided into five steps²³ (**Figure 7**):

- i. **Activation:** can be initiated by a variety of stimuli, including bone microfractures and soluble factors released in the bone microenvironment, PTH, as well as the inflammatory cytokines TNF- α , IL-1 β and IL-6 under pathological conditions. This phase turns into the activation of bone lining cells, the exposure of the bone surface and the secretion of chemokines involved in the recruitment of osteoclast precursors from the bloodstream.
- ii. **Resorption:** in this phase, osteoclasts undergo polarization and initiate acidification of the bone matrix, allowing degradation of the inorganic component, and the release of lysosomal

enzymes such as cathepsin K and MMP-9, that can degrade the organic part. From bone resorption, type I collagen degradation products are released, including terminal peptide fragments [N-terminal (NTx) and C-terminal telopeptides (CTX)], but also calcium and growth factors, such as BMP, FGF, IGF-2 and TGF- β , which trigger the subsequent recruitment of osteoblast precursors.

- iii. Reversal: the activity of osteoclasts stops, and these cells undergo apoptosis. At the same time, the bone surface becomes populated with reverse cells, macrophage-like cells responsible for the removal of residual debris produced during matrix degradation and involved in the stimulation of the anabolic activity of osteoblasts.
- iv. Formation: is the longest phase and consists in the differentiation of osteoblasts precursors, which start to secrete and deposit bone matrix, called osteoid, which is the pre-calcified bone matrix. Once hydroxyapatite crystals precipitate on osteoid, the formation phase is completed.
- v. Termination: matrix mineralization is completed, and osteoblasts undergo to their fate dying by apoptosis, becoming lining cells or remaining trapped in ECM as osteocytes.

Bone remodeling is finely regulated in order to prevent an imbalance between bone resorption and deposition. Conversely, alterations of the compensation and timing of bone resorption and formation could potentially lead to severe disorders, such as osteoporosis^{23,24}.

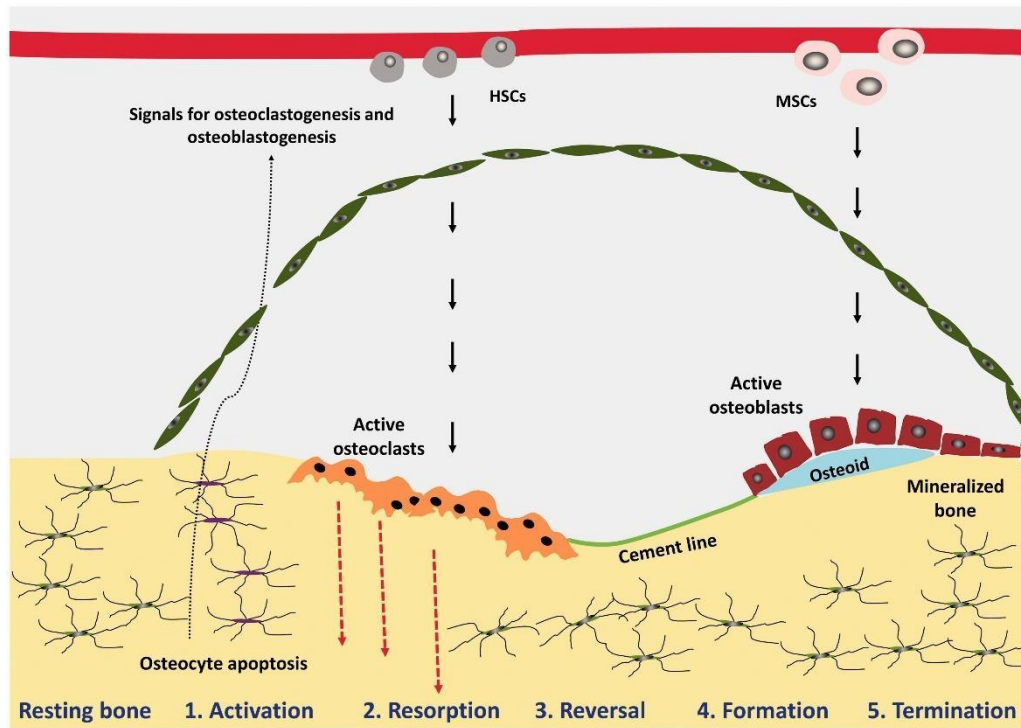


Figure 7: The Bone remodeling process. Schematic diagram of the bone remodeling cycle illustrating the phases of activation, resorption, reversal, formation and termination. Hematopoietic stem cells (HSCs) and mesenchymal stem cells (MSCs). (Source: Kenkre JS, Bassett J. 2018 ²²)

2. Osteoporosis and disuse osteoporosis

2.1 Definition

Osteoporosis is the most common metabolic bone disease, it causes decrease of bone mineral density (BMD), impaired bone microarchitecture and mineralization, and, consequently, an increase in bone fragility and risk of fracture ³⁹ (**Figure 8**). Being almost always a clinically silent disease, diagnosed only after a fracture, osteoporosis is often underrecognized and undertreated ⁴⁰. Although its etiology includes several factors, such as ageing, hormonal changes, or endocrine disorders, as well as the use of some therapies like anticonvulsant or glucocorticoids ³⁹ which reduce BMD as a side effect, osteoporosis is due to an altered balance between bone deposition and resorption functions.

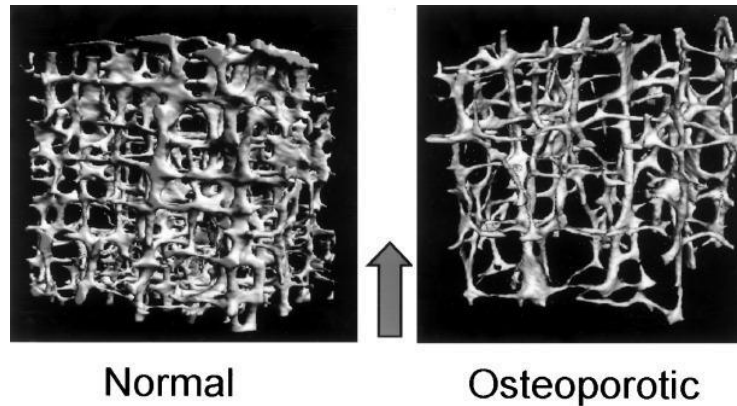


Figure 8: Normal vs osteoporotic trabecular architecture Tridimensional micro-computed tomography (μ CT) images of cadaveric vertebral biopsies from a 52-year-old woman with no osteoporosis (on the left) compared to one of an 84-year-old woman with clinically manifested osteoporosis (on the right) (Source: Borah B, Gross GJ, Dufresne TE, et al. Three-dimensional microimaging (MR μ I and μ CT), finite element modeling, and rapid prototyping provide unique insights into bone architecture in osteoporosis. *Anat Rec.* 2001;265(2):101-110. doi:10.1002/ar.1060).

Skeletal mechanical unloading or systemic immobilization result in osteoporosis, which in this case is defined as “disuse osteoporosis”⁴¹ This is a state of bone loss that occurs in different clinical conditions, including spinal cord injury, neuromuscular diseases, and immobilization, or after unloading due to weightlessness, a condition usually experienced by astronauts during space flights⁴². Bone loss during disuse is linked to a deregulation of bone-muscle crosstalk and to the lack of muscle contraction, as much as to the absence of mechanical loading, as confirmed by studies which compared the unloading effects on bone microstructure between weight-bearing bones, for instance femur or tibia, and non-weight-bearing bones, such as radius^{42, 43}. The adaptive response occurring in absence of mechanical loading is characterized by the inhibition of osteoblastic bone formation and/or by the increase of osteoclastic bone resorption, leading to bone loss⁴⁴.

2.2 Disuse osteoporosis in long-term bed rest and paralysis

Long-term bed rest, as well as paralysis due to spinal cord injury (SCI) and neuromuscular disorders (NMD), result in the absence of skeletal mechanical loading due to reduction of muscle contraction, eventually leading to osteoporosis in up to 75% of patients⁴⁹. The fracture rate is five-fold higher in patients with NMD compared to age-matched healthy people^{46, 45}. Although osteoporosis in SCI and NMD patients has been described to be caused by a combination of factors, including neuronal and hormonal changes, the main causal factor reported is the lack of mechanical loading⁴⁶. Importantly, SCI patients may not feel pain in the fracture area due to neurological damage, making the fracture difficult

to identify, which underscores the need of a better understanding of the phenomenon so that it can be more effectively prevented ⁴⁷.

Guidelines for the treatment of osteoporosis due to disuse in SCI patients include the use of both pharmacological and non-pharmacological therapies. The first recommendation involves lifestyle modification, including the cessation of detrimental behaviors such as smoking and implementation of calcium and vitamin D in the diet ⁴⁷. Mechanical loading, such as weight-bearing activity, has been demonstrated to reverse, at least partially, SCI-induced bone loss; similarly, low magnitude mechanical signals and low-intensity vibration treatment protocols have shown to be promising in bone remodeling stimulation in SCI patients. As for the available pharmacological therapies, these include the use of standard anti-osteoporotic drugs such as bisphosphonates, pharmacological compounds able to inhibit osteoclast resorption activity, or denosumab, a monoclonal antibody directed against RANKL, whose early administration allows an increase of BMD in spine and femur of SCI patients ^{47,48}.

2.3 Disuse osteoporosis in space flight

During long-duration space flights, the human body experiences a microgravity condition (μG) and undergoes adaptation phenomena. In particular, fluid mass is redistributed, and the energy required for movement is less, resulting in muscle atrophy. The cardiovascular system is fatigued, the immune system decrease, vision problems and neurological impairment can occur due to the increased intracranial pressure. Microgravity also induces skeletal adaptation, resulting in a significant bone mass reduction, increasing the risk of bone fracture and development of disuse osteoporosis ⁵⁰.

Despite preventive exercise, one of the most common problems afflicting astronauts after space flight is bone loss ⁵⁰. Astronauts can lose about 1-2% of their bone mass per month during space mission ^{51 52} and the recovery of the lost bone mass can be much longer than the mission itself ⁵³. Anti-resorptive bisphosphonates, as much as other pharmacological treatments, are effective in limiting bone loss during flight, but they may contribute to a longer and sometimes incomplete recovery⁵⁴. Changes induced in bone by microgravity conditions seem to also be different according to the site. In fact, at variance with the axial skeleton, it is possible to observe a paradoxical increase in bone mass in the skull region ⁵⁴. Whether this is due to a differential effect on muscle-loaded vs non-muscle-loaded bones remains to be understood.

Although the interest in bone health during long-duration space flights has increased since the 1960s, and it is bound to become even more of an issue with the democratization of space travel we will observe

in the future, to date microgravity-induced bone loss is still a problem and unresolved health risk for space travellers⁵⁴.

2.4 How to model simulated microgravity

As observed in astronauts, microgravity also induces bone loss in animals, especially rodents, which can therefore be used as models to study the effects of space flight on bone homeostasis^{55, 56}. Even though the experiments conducted during space flight are the most physiologically appropriate to study microgravity-induced bone loss, limitations such as the low number of space launches, the need to keep the weight of the cargo low, the number and size within certain limits of samples, as well as the complexity of experiment design and the enormous costs, prompted the researchers to develop new simulated human and animal microgravity models.

2.4.1 Simulated microgravity: human models

In order to study microgravity effects on human health, five ground-based tests have been developed: water immersion, dry immersion, unilateral lower-extremity limb suspension, head down tilt, and supine bed rest (**Figure 9**)⁵⁰.

In *water immersion* (**Figure 9a**), the volunteer is submerged from the clavicles downwards in thermoneutral water (temperature of the water: 32-34,5 °C). He floats, simulating the effect of microgravity, even if the impact is limited to the body below the neck, so it is not a perfect model for microgravity. The main limitation of this method is its duration, which cannot exceed 72 h, in fact, longer immersion in water can induce dermatitis. An additional disadvantage of this model is linked to the necessity to leave the apparatus for hygienic purposes, impacting the study.^{50, 57}

The *dry immersion* (**Figure 9b**) is very similar to water immersion, but in this case the volunteer, before being submerged in water, is covered by a waterproof high elastic cloth to keep the body dry, making this model useful for long-term studies. Floating in water leads the musculoskeletal system to experience atrophy and loss of strength similarly to those occurring in space flight during a comparable amount of time, since the reduction of bone density in lower limbs reaches 2% within 7 days⁵⁰. The longest duration for a dry immersion experiment was 56 days, while the shortest lasted 10h⁶⁸.

The *unilateral lower limb suspension* (ULLS) (**Figure 9c**) is one of the most cost-effective methods to study microgravity effects on human health and in particular on the musculoskeletal system. In ULLS, thanks to a platform shoe and crutches, one leg is held in suspension, while the other is normally weight-bearing and can be used as control. Therefore, in ULLS there is no necessity to confine the volunteer,

allowing him to travel, work or stay at home. Even though this model is useful for studying the effect of unloading on muscles and bone, it is not possible to study whole body or cardiovascular changes ⁵⁰.

The *supine bed rest* (SBR **Figure 9d**) provides a uniform fluid distribution throughout the body, which together with the lack of mechanical loading leads to effects similar to those induced by microgravity. However, this method also results in the compression of posterior tissues, which does not happen in microgravity conditions. In order to overcome this limitation, the head-down tilt bed rest was developed.

The main goal of the *head-down tilt bed rest* (HDTBR **Figure 9e**) is to reproduce on Earth the conditions experienced by the human body during space flight, in particular the absence of hydrostatic pressures and the equal distribution throughout the body of the arterial pressure. Subjects are placed in supine position on a bed that is tilted 6 degrees, to place the head closer to the ground and elevate the feet. As opposed to supine bed rest, HDT increases head-ward fluid shifts but alters the gravity vector over the entire body from front to back. For the method to work, the subject cannot leave the position even for a short period or use a pillow. This posture does not completely remove the application of gravity and therefore it does not completely simulate the effect of microgravity environment, even if HDT leads to a decrease in bone density ⁵⁰.

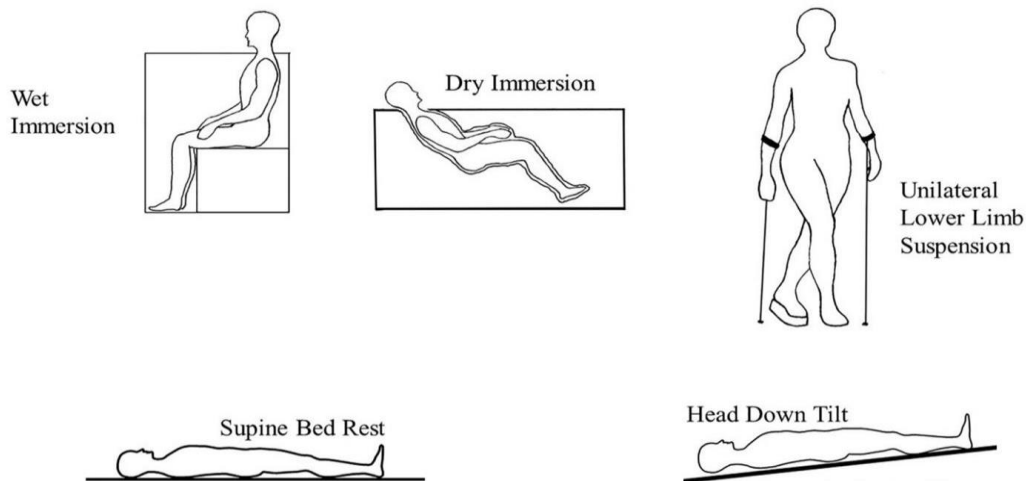


Figure 9: Microgravity ground-based models in human Diagram illustrating tests for microgravity ground-based study in humans. (Source: adapted from Pandiarajan, M., & Hargens, A. R. (2020) ⁵⁰).

2.4.2 Simulated microgravity: animal models

The effects of the disuse in animal models can be studied by unilateral or bilateral immobilization of the hindlimbs.

As for unilateral *immobilization*, it is possible to use a bondage to fix one of the hindlimb of the rodent, thus preventing its movement but allowing for any other movement of the 3 remaining limbs. Immobilization of the hindlimb results in a substantial loss of muscle and bone mass, and in a deterioration of the trabecular microarchitecture, making this model useful for studying the effects of microgravity on musculoskeletal apparatus but not on other organs. The contralateral, non-immobilized hindlimb is a great control, albeit the effect of increased loading should be considered in the analyses and therefore standard caged animals should also be kept as control in these experiments if possible ⁵⁸. Moreover, the fact that the immobilized hindlimb still has functional muscles may allow for some loading to still occur on the bones, which can increase the variability. Unilateral hindlimb immobilization in mice is normally performed on eight/ten-week-old male mice. Animals are anesthetized and their left hind limb is shaved and wrapped with surgical tape from the paw to the knee. A microcentrifuge tube with the bottom end removed, in order to allow air flow into it, is fixed on the tape immobilizing the hindlimb. The duration of the experiments is generally three weeks ⁶⁹.

A model that provides similar outcomes in terms of monolateral hindlimb immobilization is the botulin toxin A (botox) injection ⁵⁹. The recommended botox dose for mice is 2 international units (IU) per 100g body weight, to be injected into the *quadriceps femoris* and the *gastrocnemius* muscles. Injection of botox in both these muscle groups determines a uniform flaccid paralysis and hindlimb disuse. The duration of the experiment is usually of three weeks, at the end of which muscle and bone degradation occurred in response to the muscle paralysis can be observed ^{69, 70}.

The best animal model chosen to study the effect of microgravity on bone tissue is represented by hindlimbs suspension (HLS) by tail traction ⁶⁰. In this method, a strip of elastic tape is applied to the ventral surface of the tail, making a half-circle at the centre and fixed by another strip of the tape applied spiral to the whole tail. Through a swivel, the half-circle of tape is fixed to an overhead wire, whose height is adjusted to maintain the animals suspended at an approximately 30°. This apparatus allowed animals access to food and water and to move freely into the cage using their forelimbs ⁷¹.

The optimum angulation between the animal's body and the bottom of the cage is 30° and is necessary to prevent excessive orthostatic intolerance and stress to the animal ⁶⁰ (**Figure 10**). Several studies confirmed that HLS results in a significant reduction of bone, mostly due to an increase in bone resorption, rather than to a decrease in bone formation ^{61, 71, 25, 26}.

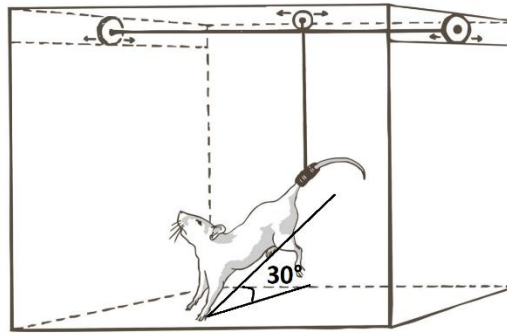


Figure 10: Simulate microgravity: hindlimbs suspension by tail traction. This animal model is used to study spaceflight like changes in rats and mice, suspending rodents through the tail. The forelimbs stay on the bottom of the cage and allow the animal to move around freely to reach food and water, while the hindlimbs remain suspended and do not touch the ground. To prevent excessive orthostatic intolerance and stress, the angulation between the animal's body and the bottom of the cage should be 30°. (Source: adapted from <https://gaidi.ca/weblog/a-dynamic-hindlimb-unloading-apparatus/>)

2.4.3 Simulated microgravity: *in vitro* models

Although the microgravity conditions achieved in space cannot be perfectly replicated on Earth, scientists have developed bioreactors that allow them to mimic the effects of microgravity *in vitro* ⁶².

One of these bioreactors is the *Rotating-wall vessel (RWV)*, which is a cylindrical, horizontally-rotating bubble free bioreactor, with an inner co-rotating cylinder with a gas exchange membrane. Cells and liquid culture media are placed in the space between the inner and the outer cylinders, and the assembled device is rotated about its longitudinal axis at constant speed. The culture medium, and the cells on microcarriers, rotate inside the vessel in a low-shear, low-turbulence and low fluid stress forces environment. Microcarriers are in suspension and rotate inside the vessel of the bioreactor as a solid body. The horizontal rotation of the vessel subjects the cells to a randomization of the normal gravity vector, thus mimicking a state of simulated free fall (Figure 11). To culture cells usually maintained in adhesion, gelatin microcarriers beads are used as substrate for adhesion ^{72, 74}. Although the environment generated inside the vessel is low-shear, the shear stress is not null, and it may affect cellular behavior and differentiation ⁶².

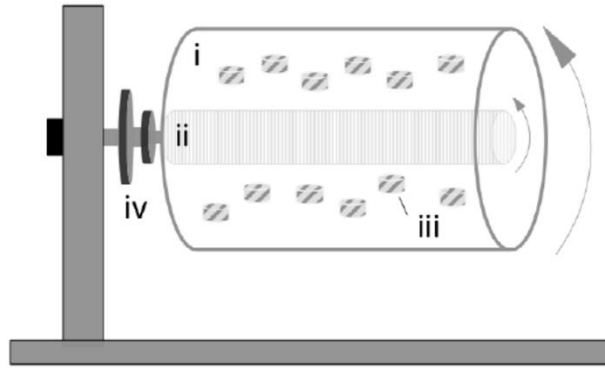


Figure 11: Schematic representation of the rotating-wall vessel (RWV) bioreactor. It is composed of (i) Outer and (ii) inner cylinders, (iii) cell constructs and (iv) rotator base. Rotating wall vessels are filled with culture medium and medium oxygenation is provided via a silicone-rubber gas-transfer membrane. Cells are cultured in a microgravity environment. (Source Bioreactor Systems for Human Bone Tissue Engineering - Scientific Figure on ResearchGate. Available from: https://www.researchgate.net/figure/Rotating-wall-vessel-Schematic-representation-of-a-rotating-wall-vessel-showing-the_fig2_272660002)

Another kind of bioreactor used to simulate microgravity on ground is the *Random positioning machine (RPM)*. This machine consists of a culture chamber mounted on a rotating platform with two independent rotating frames, whose direction changes continuously and randomly, nullifying the gravity vector of the earth. RPM can be controlled to achieve a randomized gravity vector, allowing for more representative microgravity simulations. Nevertheless, the sheer forces and vibrations generated by this system can influence cell behavior, and the limited size of the culture chamber can be a limit to the type of experiments that can be performed ⁶³.

Two-dimensional (2D)-Clinostat consists of a platform that can rotate samples in two dimensions, along a single axis, so that gravitational forces act equally in all directions. Even if it cannot replicate exactly the microgravity condition experienced in space, it constitutes an excellent tool for the study of simulated microgravity *in vitro*, especially due to the simplicity with which it can be designed, operated, and maintained. Unfortunately, the 2D rotation cannot eliminate completely the effects of gravity on the samples, thus some gravitational artefacts or uneven force distributions can affect the accuracy of the results. In addition, two-dimensional rotation limits the orientations and configurations of the tested sample ⁶².

Three-dimensional (3D)-Clinostat consists of a platform capable of rotating samples in three dimensions around two perpendicular axes, at a constant speed. This rotation makes gravitational forces null on the samples, simulating the unloading conditions experienced in space. Unlike the 2D clinostat, this system is difficult to use, and requires technical expertise for the design and use, as well as additional

hardware and software components, which make this technique more expensive. Anyway, the 3D rotation provides a more accurate microgravity simulation than the 2D version ⁶².

3. Aim of the work

When bone is challenged by disuse, its physiological balance is perturbed, such as in the case of mechanical unloading due to forced bed rest or long duration space flights ⁵⁰. This causes inhibition of osteoblastic bone formation and the increase of osteoclastic bone resorption, leading to bone mass decrease which can result in disuse osteoporosis ⁵⁰. It is of paramount importance to understand the molecular mechanisms leading to this disease, so that it can be combated or prevented in a more effective way.

In a whole gene expression profiling analysis performed in osteoblasts subjected to microgravity as a model of mechanical unloading, we found *Penk1* (Pre-proenkephalin 1) and *Lcn2* (Lipocalin 2) to be the most down and up-regulated genes, respectively ³³. *Penk1* is a gene encoding a pro-neuropeptide that is proteolytically processed to generate the following enkephalins: [Met]-enkephalin, [Met]-enkephalin extended sequence and [Leu]-enkephalin, all belonging to the family of opioid peptides that are endogenous ligands for opioid receptors having potent analgesic properties ^{27, 28, 31}. Dysfunction of the enkephalin system has been implicated in a range of psychiatric and neurological disorders, in chronic pain, cardiac and gastrointestinal functions, and in immunity ³². *Lcn2* is a gene encoding for the glycoprotein Lipocalin-2 (LCN2), also known as Neutrophil Gelatinase-Associated Lipocalin (NGAL) ^{33, 34}. LCN2 is a circulating protein, is expressed in a huge variety of cells, including hepatocytes, lung, bone marrow, macrophages, thymus, prostate, kidney and even in bone and is involved in several functions ³⁵.

These two genes were not known to be associated with bone cell functions, thus representing new potential targets and/or biomarkers for low mechanical loading in bone. The present PhD thesis is aimed at more deeply understand whether *Penk1* and *Lcn2* may be involved in osteoblasts' response to mechanical unloading.

In particular, in **Chapter 2** we conducted a study aimed at investigating *Penk1* involvement in bone metabolism under physiological and mechanical unloading conditions. In **Chapter 3**, instead, we analyzed the effect of genetical ablation of *Lcn2* on osteoblasts subjected to simulated microgravity.

In **Chapter 4** the general conclusions of this thesis are presented and in **Chapter 5** are reported the references of this thesis. Lastly in **Chapter 6** are presented the achievement.



Chapter 2: “Pre-proenkephalin 1 is downregulated under unloading and is involved in osteoblast biology”

Published in Calcified tissue international, 2024 (doi: 10.1007/s00223-024-01199-z.)

Puri C, Dannenberg C, Ucci A, Ponzetti M, Pucci E, Silvestri L, Lau P, Frings-Meuthen P, Heer M, Rucci N, Teti A, Maurizi A.

1. Abstract

Pre-proenkephalin 1 (PENK1) is a pro-neuropeptide that belongs to the typical opioid peptide's family, having analgesic properties. We found *Penk1* to be the most downregulated gene in a whole gene profiling analysis performed in osteoblasts subjected to microgravity as a model of mechanical unloading. In this work, *Penk1* downregulation was confirmed in the bones of two *in vivo* models of mechanical unloading: tail suspended and botulinum toxin A (botox)-injected mice. Consistently, in the sera from healthy volunteers subjected to bed rest, we observed an inverse correlation between PENK1 and bed rest duration. These results prompted us to investigate a role for this factor in bone. *Penk1* was highly expressed in mouse bone, but its global deletion failed to impact bone metabolism *in vivo*. Indeed, *Penk1* knock out (*Penk1*^{-/-}) mice did not show an overt bone phenotype compared to the WT littermates. Conversely, *in vitro* *Penk1* gene expression progressively increased during osteoblast differentiation and its transient silencing in mature osteoblasts by siRNAs upregulated the transcription of the *Sost1* gene encoding sclerostin, and decreased *Wnt3a* and *Coll1a1* mRNAs, suggesting an altered osteoblast activity due to an impairment of the Wnt pathway. In line with this, osteoblasts treated with the *Penk1* encoded peptide, Met-enkephalin, showed an increase of *Osx* and *Coll1a1* mRNAs and enhanced nodule mineralization. Interestingly, primary osteoblasts isolated from *Penk1*^{-/-} mice showed lower metabolic activity, ALP activity and nodule mineralization, as well as a lower number of CFU-F compared to osteoblasts isolated from WT mice, suggesting that, unlike the transient inhibition, the chronic *Penk1* deletion affects both osteoblast differentiation and activity. Taken together, these results highlight a role for Penk1 in the regulation of the response of the bone to mechanical unloading, potentially acting on osteoblast differentiation and activity in a cell autonomous manner.

2. Introduction

Recent research has shown that neuropeptides affect the functions of bone cells playing an essential role in the metabolism of the skeletal tissues^{31,32}. Pre-proenkephalin 1 (*Penk1*) is a gene encoding a pro-neuropeptide that is proteolytically processed to generate the following enkephalins: [Met]-enkephalin, [Met]-enkephalin extended sequence and [Leu]-enkephalin, all belonging to the family of opioid peptides that are endogenous ligands for opioid receptors having potent analgesic properties⁷⁶. In addition to their analgesic effects, enkephalins also regulate mood, stress, and addiction⁷⁷. Dysfunction of the enkephalin

system has been implicated in a range of psychiatric and neurological disorders, in chronic pain, cardiac and gastrointestinal functions, and immunity⁷⁸⁻⁸³. Coherently with the broad range of functions, their expression is not limited to the nervous and neuroendocrine systems. Indeed, *Penk1* mRNA is particularly abundant during development⁸⁴ and is expressed in many tissues, such as kidney, liver, lung, skeletal muscle, and heart^{85, 86}.

Our interest in *Penk1* started from a previous study of global gene profiling analysis performed in mouse primary osteoblasts subjected to simulated microgravity by employing the NASA-developed Rotating Wall Vessel (RWV) apparatus as an *in vitro* model of mechanical unloading⁷⁴. Among the differentially regulated genes observed in this study, some were not known to be associated with bone cell functions, thus representing new bone determinants. These included *Penk1*, which resulted to be the most downregulated osteoblast mechano-responding transcript in our experimental conditions⁷⁴. Indeed, previous studies already demonstrated the expression of *Penk1* in bone and joints^{87, 88}. Moreover, Rosen et al. identified *Penk1* mRNA in foetal rat calvaria-derived cells as well as in osteoblast-like cell lines^{97, 89}. The same authors reported an inverse correlation between osteoblastic *Penk1* mRNA levels and cellular differentiation⁹⁰. Later, Seitz *et al.*⁹¹ found that, at variance with Rosen finding, *Penk1* was more expressed in differentiated osteoblasts, but its presence seemed to be dispensable for bone development, since bone histomorphometry did not reveal any bone defect in a mouse model deficient for *Penk1*^{91, 92}. However, when *Penk1* was deleted in a spontaneous mouse model recapitulating the X-linked hypophosphatemic rickets disease (i.e. Hyp mouse), which harbours a deletion within the *PheX* gene encoding for an endopeptidase crucial for bone mineralization, they observed a reduction of the osteoid enrichment at 24 weeks of age⁹¹. Interestingly, Pérez-Castrillón and colleagues⁹³ found the expression of opioid receptors in the osteoblast-like MG63 cell line, suggesting the ability of these cells to respond to opioid stimulation.

Overall, the relationship between *Penk1* and bone metabolism is still an area of active research. In this context, we sought to investigate *Penk1* involvement in bone metabolism under physiological and mechanical unloading conditions. We confirmed, in *in vivo* mouse and human models, an inverse correlation between *Penk1* and unloading. However, we could not find any obvious phenotype in *Penk1*^{-/-} mice. In contrast, in *ex vivo* osteoblast primary cultures the lack of *Penk1* impaired Alkaline phosphatase (Alp) activity and nodule mineralization formation. Consistently, transient *Penk1* knock-down in differentiated osteoblasts by siRNAs treatment reduced the transcriptional expression of genes involved in bone formation, while treatment with the opioid receptor agonist Met-Enkephalin (Met-Enk) encoded by *Penk1* increased the transcriptional expression *Collagen 1a1* as well as nodule mineralization.

3. Materials and methods

3.1 Materials

Dulbecco's modified Minimum Essential Medium (DMEM), penicillin, streptomycin, and trypsin were from Euroclone (Milan, Italy), Fetal Bovine Serum (FBS) was from GIBCO (Uxbridge, UK). Sterile plastic ware was from Greiner bio-one (Kremsmünster, Austria) or Euroclone (Milan, Italy). TRIzol reagent (cat#15596018), primers and reagents for RT-PCR (cat#k1622) were from Invitrogen (Carlsbad, CA, USA). The qRT-PCR assays Luna Universal One-Step RT-qPCR Kit (#E3006) was from New England Biolab. Human (cat#CSB-EL017781HU) and mouse (cat#CSB-EL017781MO) PENK1 ELISA assays were from Cusabio (Houston, TX, USA); Carboxy Terminal collagen crosslinks (CTx, cat#AC-06F1), Procollagen type I N-terminal Propeptide (PINP1, cat#AC-33F1) and Tartrate-Resistant Acid Phosphatase (TRAcP, cat#SB-TR103) immunoenzymatic kits were from Immunodiagnostic Systems (The Boldons, UK). Met-Enkephalin (Met-Enk) was purchased by Sigma (cat# M6638). Anti-Collagen I α 1 antibody was from Immunological Sciences (cat#AB82138). All other reagents, including the histochemical Alp (cat #86C-1KT) and TRAcP (cat #386) kits, and Thiazolyl Blue Tetrazolium Bromide (cat# M2128), were of the purest grade from Sigma Aldrich Co. (St. Louis, MO, USA). ON-TARGETplus Mouse Penk1-siRNA SMARTpool was purchased from Dharmacon (#L-050124-00-0005).

3.2 Animals

Penk1^{-/-} mice (background C57BL/6J) were purchased by the European Mouse Mutant Archive (EMMA), and their phenotype described in König *et al.*⁹². They are vital, with an overall normal lifespan and fertility. All procedures involving animals and their care were conducted in conformity with national and international laws and policies (European Economic Community Council Directive 86/609, OJ L 358, 1, December 12, 1987; Italian Legislative Decree 4.03.2014, n.26, Gazzetta Ufficiale della Repubblica Italiana no. 61, March 4, 2014) and animal procedures received approval by the Italian Ministry of Health authority (Approval N. 392/2020-PR). Mice were housed in the animal facility of the University of L'Aquila, Italy, at the following conditions: temperature: 20-24°C, humidity: 60%, dark/light cycle: 12/12 hours. They had access to food and water *ad libitum* and were fed with standard diet (Mucedola code: 4RF21).

3.3 Hindlimb suspension and in vivo treatment with botulin toxin A

Hindlimb suspension (HLS) was performed according to Sakata *et al*⁹⁴ on 8-week-old C57BL/6J male mice and as described in Rucci *et al.*⁷¹ while *in vivo* treatment with botulinum toxin A (Botox) was performed in 8-week-old C57BL/6J male mice according to Warner and colleagues⁷⁰ and as described in Rucci *et al.*⁷¹.

3.4 Head Down tilt Bed Rest (HDBR) experiment

A 14-day head-down tilt bed rest (HDBR) study, including 8 male subjects (mean age 26.3 ± 3.5 years, Body Weight [BW] 78.0 ± 4.3 kg) was conducted in the metabolic ward of the German Aerospace Center. Immobilization was accomplished with 6-degree HDBR, a valid ground-based model to simulate microgravity-induced bone loss. Study design and primary outcome are described more detailed in Frings-Meuthen and colleagues⁹⁵. For the assessment of serum PENK1 levels in the present study, we took advantage of 3 unutilized study samples. Approval for the study was obtained from the Ethical Committee of the “Aerztekammer Nordrhein,” Düsseldorf, Germany, and was conducted in accordance with the latest version of the Declaration of Helsinki. The study is registered on <http://www.clinicaltrials.gov> with the unique trial number: NCT01183299; registration date: August 13, 2010.

3.5 Osteoblast primary cultures

Primary mouse osteoblast cultures were performed according to Capulli *et al.*³³ and cells were cultured in DMEM plus 10% FBS. At confluence, cells were trypsinized and plated according to the experimental protocol.

For siRNA transfection, mouse primary osteoblasts (1×10^6 cells) were nucleofected with 100nM of *Penk1*-specific or scrambled (SCR)- siRNA (Dharmacon) using the Amaxa Mouse Neuron Nucleofector kit (Lonza, Basel, Switzerland; Cat. #VPG-1001). After 48 hours from nucleofection, osteoblasts were employed for the experiments. Alp activity was evaluated cytochemically according to the manufacturer’s instructions. For mineralization assay, DMEM plus 10% FBS was supplemented with 10mM β -glycerophosphate and 50 μ g/mL ascorbate (osteogenic medium). Mouse primary osteoblasts were cultured for 3 weeks before evaluation of mineralization nodules by von Kossa staining. Metabolic activity was assessed by the 3-(4,5-dimethylthiazol-2-yl)-2,5-diphenyltetrazolium (MTT) bromide reduction assay, according to the manufacturer’s instructions.

Alp-positive colony forming unit (CFU) was performed according to Capulli *et al.*³³ and at the end

of the experiment number and area of Alp-positive colonies were analyzed to estimate the amount of osteoblast progenitors in the bone marrow, using the Fiji® software.

3.6 Comparative real-time RT-PCR

Total RNA was extracted Using the TRIzol® method. One microgram of RNA was reverse transcribed into cDNA using Revert Aid First Strand cDNA Synthesis Kit (Invitrogen) and the equivalent of 0.1 µg was processed using the Luna Universal One-Step RT-qPCR Kit (New England Biolab). Results, expressed as fold increase *versus* control, were normalized with the housekeeping gene glycerol-3-phosphate dehydrogenase (*Gapdh*). Primer sequences are reported in Table 1.

Table 1: Real time primers sequences

Gene	Forward primer	Reverse primer
<i>Gapdh</i>	5'-TGTGAGGGAGATGCTCAGT-3'	5'-TGTTCTACCCCCAATGTG-3'
<i>Penk1</i>	5'-GACAGCAGCAAACAGGATGA-3'	5'-GTTGTCTCCCGTCCAGTA-3'
<i>Akp2</i>	5'-CCAGCAGGTTTCTCTCTGG-3'	5'-CTGGGAGTCTCATCCTGAGC-3'
<i>Runx2</i>	5'-CCCAGCCACCTTACCTACA-3'	5'-TATGGAGTGCTGCTGGTCTG-3'
<i>Osx</i>	5'-TGCTTCCCAATCTATTTGC-3'	5'-AGAATCCCTTCCCTCTCCA-3'
<i>Coll1a1</i>	5'-CACCTCAAGAGCCTGAGTC-3'	5'-GTTCCGGCTGATGTACCAGT-3'
<i>Bglap</i>	5'-TTCTGCTCACTCTGCTGACC-3'	5'-GGGACTGAGGCTCCAAGGT-3'
<i>Sost</i>	5'-ACAAGGATGGGAGGTGACTG-3'	5'-ACCCCGTGTAGACTGGTGAG-3'
<i>RankL</i>	5'-AGCCGAGACTACGGCAAGTA-3'	5'-CCACAATGTGTTGCAGTTCC-3'
<i>Opg</i>	5'-AGTCCGTGAAGCAGGAGTG-3'	5'-CCATCTGGACATTTTTTGCAA-3'
<i>Il-1β</i>	5'-GCCCATCCTCTGTGACTCAT-3'	5'-AGGCCACAGGTATTTGTGCG-3'
<i>Il-6</i>	5'-GTTCTCTGGAAATCGTGGA-3'	5'-GGAAATTGGGTAGGAAGGA-3'
<i>Wnt3a</i>	5'-TACCCGATCTGGTGGTCCTT-3'	5'-GGGCATGATCTCCACGTAGT-3'

3.7. MicroCT analysis

Images of femurs previously fixed in 4% buffered paraformaldehyde were acquired using the SkyScan 1174 (Bruker, Billerica, MA, USA) with a resolution of 6.7µm (X-ray voltage 50 kV). Image reconstruction was carried out employing a modified Feldkamp algorithm using the Skyscan Nrecon software. Three-dimensional (3D) and two-dimensional (2D) morphometric parameters were calculated for the trabecular bone, 100 slides (6.7µm thick) from the growth plate⁹⁶. 3D parameters were based on analysis of a Marching Cubes-type model with a rendered surface^{97,98}. Calculation of all 2D areas and

perimeters was based on the Pratt algorithm⁹⁹. Bone structural variables and nomenclature were those suggested by Bouxsein et al. (2010)¹⁰⁰. Cortical bone thickness was analyzed 450 slides below the growth plate on 54 slides as described in Rufo *et al.*¹⁰¹.

3.8 Bone histomorphometry

Tibiae harvested from WT and *Penk1*^{-/-} mice were fixed in 4% buffered paraformaldehyde, dehydrated in ascending alcohol series, and processed for methyl–methacrylate embedding without decalcification. Histomorphometric measurements were carried out on 5- μ m-thick sections using the image analysis software NIH ImageJ (RRID:SCR_003070 version 1.50i.) and with the suggested nomenclature¹⁰². Osteoclast number/bone surface (Oc.N/BS) and osteoclast surface/bone surface (Oc.S/BS%) were evaluated after histochemical staining for TRAcP activity, while osteoblast number/bone surface (Ob.N/BS) and osteoblast surface/bone surface (Ob.S/BS%) were evaluated in sections stained with toluidine blue. Dynamic assessment of the mineral apposition rate (MAR) was calculated after double injection of calcein, 10 and 3 days before euthanasia. Bone formation rate (BFR) was calculated according to the following formula: $MAR \times MS/BA$, where MS = mineralized surface and BA = bone area, as suggested by Dempster and colleagues¹⁰².

3.9 Bone turnover biomarkers

Markers of bone turnover, including CTx, TRAcP 5b isoform and PINP1 were evaluated in sera collected from WT and *Penk1*^{-/-} mice by ELISA according to the manufacturer's instructions.

3.10 Statistics

Results are expressed as the mean \pm SD of at least 3 independent experiments, 3 human subjects, and at least 4 mice/group. Statistical analyses were performed by the Student's *t* test or linear regression test according to the type of data, using the Prism Graph pad software (v8). A p-value <0.05 was conventionally considered statistically significant.

4. Results

4.1 Mechanical unloading induces *Penk1* downregulation in mouse and human

Our interest in *Penk1* started from a previous work showing, by a whole genome microarray assay, that it was the most downregulated gene in osteoblasts subjected to microgravity as a model of *in vitro* mechanical unloading⁷⁴, suggesting a possible involvement of *Penk1* in the osteoblast mechano-response. These results prompted us to evaluate *Penk1* expression in two mouse models of disuse osteoporosis due to mechanical unloading: the tail suspended mice and mice injected with botox in the right quadriceps and the posterior compartment of the right calf. Interestingly, we observed a significant reduction of *Penk1* mRNA expression in the femurs of mice subjected to hindlimb suspension (HLS) compared to mice maintained in normal loading condition (NLC, **Figure 1a**). Consistently, a decrease of *Penk1* mRNA was also observed in the botox-injected hindlimbs, *versus* the contralateral limbs injected with vehicle (**Figure 1b**). Moreover, we had the chance to evaluate PENK1 expression in human sera from healthy volunteers subjected to bed rest for 14 days, a well-known mechanical unloading model. Our analysis showed a significant reduction of PENK1 serum level after 14 day of bed rest (**Figure 1c**) along with an inverse correlation between PENK1 serum levels and duration of bed rest (**Figure 1d**). Taken together, these results indicate that mechanical unloading causes a reduction of *Penk1* expression systemically, as observed in humans, or locally in bone, as observed in mice, and this could mediate the response of the skeleton to this condition.

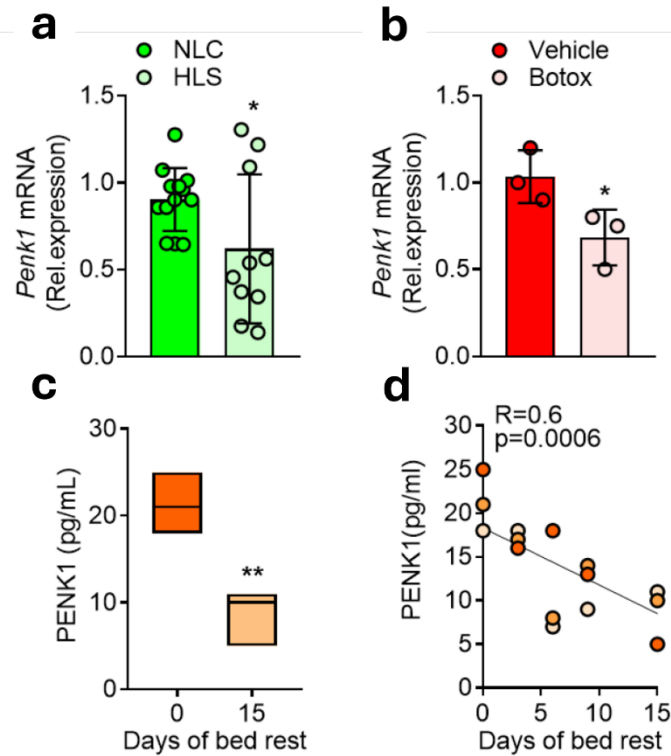


Figure 1: Penk1 modulation in mouse and human models of unloading. (a) Eight-week-old male mice were maintained in normal loading condition (NLC) or were subjected to hindlimb suspension (HLS) for 21 days. Transcriptional expression of *Penk1* in femurs by comparative real-time RT-PCR. (b) Eight-week-old mice were injected with saline solution (vehicle) or with Botulinum toxin A (Botox, 20 μ L of 2.0 unit/100 g), into the right quadriceps and the posterior compartment of the right calf (targeting gastrocnemius, plantaris, and soleus) of the left or the right hindlimbs, respectively. Transcriptional expression of *Penk1* in femurs by comparative real-time RT-PCR. (c) Serum PENK1 was assessed by ELISA in the sera of human healthy volunteers at time 0 and after 14 days of bed rest. (d) Linear regression test showing an inverse correlation between serum PENK1 levels of human healthy volunteers subjected to bed rest and the duration of unloading. In (a,b) results are the mean \pm SD of 3-10 mice/group. * $p \leq 0.05$ (Student's t test). Results in (c) are the mean \pm SD of 3 human subjects per group. ** $p = 0.01$ (Student's t test).

4.2 Lack of an overt bone phenotype in *Penk1* KO mice.

Based on the effect of the microgravity on *Penk1* expression, we aimed at characterizing the role of *Penk1* *in vivo*. Interestingly, besides the brainstem and the cerebellar cortex, already expected to express *Penk1* mRNA, we found a comparable transcriptional expression of this gene in mouse femurs and calvariae cleaned from bone marrow, while its expression in the flush-out bone marrow cells was very low (**Figure 2a**). Further examination revealed that, among the bone cells evaluated, the osteoblasts

expressed significantly higher transcriptional and protein levels of *Penk1* compared to osteoclasts (**Figure 2b,c**).

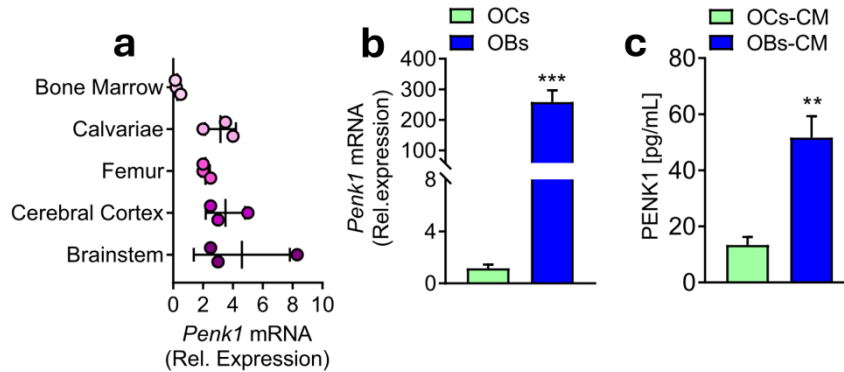


Figure 2: *Penk1* expression. (a) Transcriptional expression of *Penk1* evaluated by real time RT-PCR in the indicated organs and tissues collected from 3-month-old WT male mice. (b) Transcriptional expression of *Penk1* in mouse primary osteoclasts (OCs) and osteoblasts (OBs). (c) *Penk1* protein levels in conditioned medium harvested from mouse osteoclast (OCs-CM) and osteoblast (OBs-CM) primary cultures. Gene expression was normalized using mouse *Gapdh*. Data are the mean \pm SD of at least 3 mice or 3 cell preparations per group. ** $p=0.0012$; *** $p\leq 0.001$. (Student's t).

However, in line with Seitz *et al.*⁹¹, μ CT analysis on tibiae of *Penk1*^{-/-} mice did not show any difference in bone volume over tissue volume between the two genotypes at 3 and 12 months of age in male mice (**Figures 3a**). Consistently, evaluation of trabecular parameters showed that the trabecular number (Tb.N, **Figures 3b**), thickness (Tb.Th, **Figures 3c**) and separation (Tb.Sp, **Figures 3d**), as well as the cortical bone thickness (Ct.th, **Figures 3e**), were not influenced by the lack of *Penk1*. As expected, histomorphometry revealed that osteoclast number/bone surface (Oc.N/BS), osteoclast surface/bone surface (Oc.S/BS %), osteoblast number/bone surface (Ob.N/BS) and osteoblast surface/bone surface (Ob.S/BS%) were similar between the two genotypes (**Figures 4a-d**), along with the bone dynamic parameters Mineral Apposition Rate (MAR) and Bone Formation Rate (BFR) (**Figures 4e, f**), both in males and females. Similar results were obtained for females (**Table 2**). Finally, no differences were observed in the serum bone remodeling biomarkers TRAcP, CTx and P1NP (**Table 3**). Therefore, despite the results we found in microgravity, these data confirmed that the systemic ablation of *Penk1* *in vivo* does not affect bone metabolism in normal mechanical conditions. These results can be partially explained by the combined effect of residual enkephalins and other neuropeptides on bone cells that could potentially counterbalance the effect of the absence of *Penk1* *in vivo*.

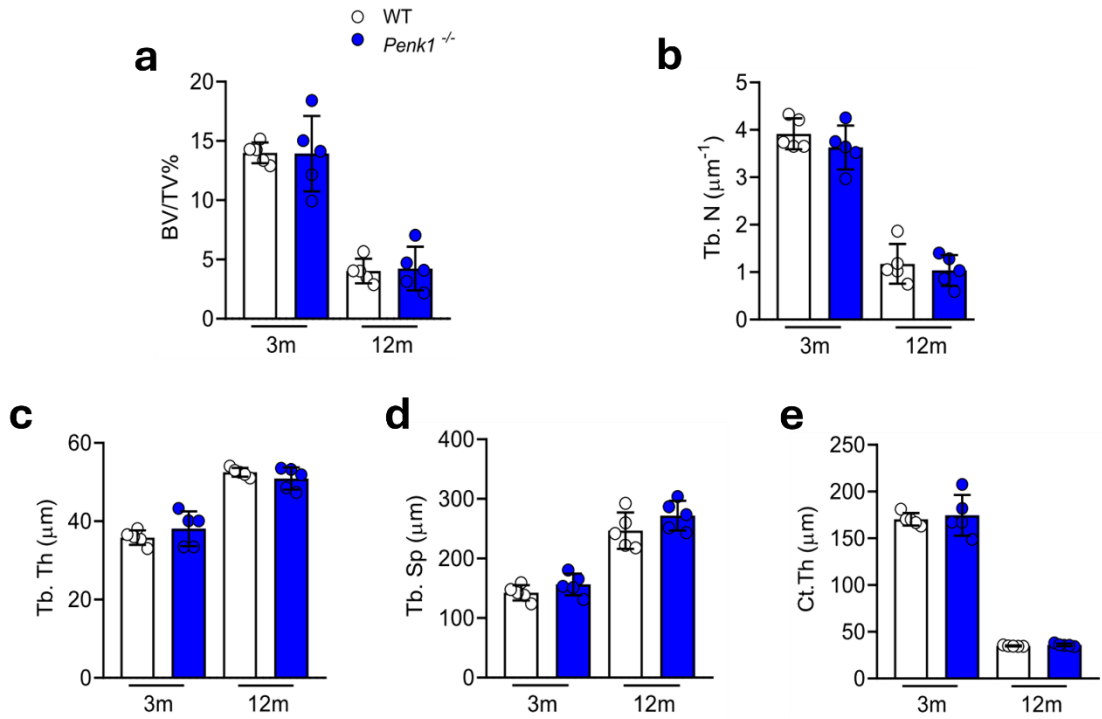


Figure 3: Bone phenotype of *Penk1* globally deleted mouse model. MicroCT analysis of distal femurs isolated from 3 and 12-month-old WT and *Penk1*^{-/-} male mice to evaluate (a, e) trabecular and cortical bone structural variables. Data are the mean ±SD of 5 mice per group. (Student's t).

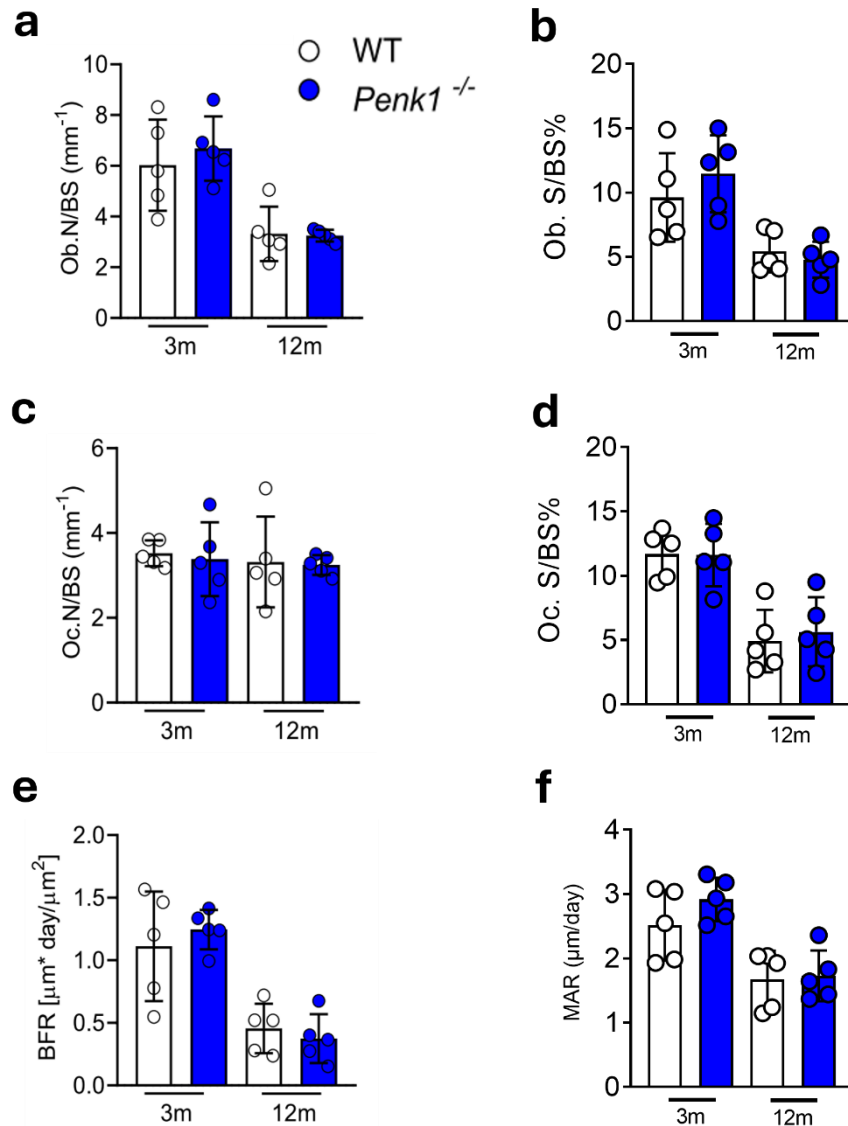


Figure 4: Bone histomorphometric analyses of *Penk1* globally deleted mouse model. Histomorphometry performed on histological sections of tibiae isolated from 3 and 12-month-old WT and *Penk1*^{-/-} male mice, stained with toluidine blue to evaluate (a) osteoblast number per bone surface (Ob.N/BS) and (b) osteoblast surface per bone surface (Ob.S/BS%), and stained for Tartrate-resistant acid phosphatase (TRAcP) activity to assess (c) osteoclast number per bone surface (Oc.N/BS) and (d) osteoclast surface per bone surface (Oc.S/BS%). Mice were subjected to a double injection (10 and 3 days prior sacrifice) of calcein in order to evaluate the following dynamic parameters: (e) Bone Formation Rate (BFR) and (f) Mineral Apposition Rate (MAR) Data are the mean ±SD of 5 mice per group. (Student's t).

Table 2: Bone microarchitectural and histomorphometric parameters in 3 and 12-month-old WT and *Penk1*^{-/-} female mice

	3-month-old			12-month-old		
	WT	<i>Penk1</i> ^{-/-}	p value	WT	<i>Penk1</i> ^{-/-}	p value
Trabecular bone, μCT						
BV/TV%	8.39	8.59	0.79	1.83	1.07	0.07
Tb.N (μm^{-1})	0.0025	0.0025	0.89	0.36	0.23	0.08
Tb.Th (μm)	33.59	35.03	0.43	49.97	44.04	0.12
Tb.Sp (μm)	197.15	197.09	1.00	402.36	398.35	0.90
Cortical bone, μCT						
Ct.Th (μm)	185.08	184.63	0.90	36.33	34.84	0.22
Trabecular bone, histomorphometry						
Oc.S/BS, %	12.56	11.53	0.60	6.26	5.87	0.64
Oc.N/BS (mm^{-1})	4.96	4.96	1.00	1.77	2.27	0.28
Ob.S/BS, %	9.22	8.39	0.55	5.09	4.61	0.34
Ob.N/BS (mm^{-1})	5.57	5.29	0.71	3.63	3.49	0.66
BFR ($\mu\text{m}^2/\mu\text{m}/\text{day}$)	1.19	1.1710	0.95	0.47	0.39	0.25
MAR ($\mu\text{m}/\text{day}$)	3.2817	3.6248	0.62	1.15	0.99	0.07

Table 3: Serum bone remodeling biomarkers in WT and *Penk1*^{-/-} mice

	Males			Females		
	WT	<i>Penk1</i> ^{-/-}	p value	WT	<i>Penk1</i> ^{-/-}	p value
3-month-old						
TRAcP (U/L)	7.17	8.70	0.15	7.96	7.97	0.99
CTx (ng/ml)	12.22	15.12	0.50	27.55	33.62	0.18
PINP (ng/ml)	35.31	67.36	0.13	46.6	38.80	0.58
12-month-old						
TRAcP (U/L)	2.25	2.31	0.94	4.07	3.84	0.82
CTx (ng/ml)	19.74	17.04	0.43	22.17	21.32	0.76
PINP (ng/ml)	47.29	53.07	0.81	41.90	61.66	0.29

4.3 *Penk1* regulates osteoblast differentiation and activity.

To remove any confounding effect related to compensatory mechanism acting *in vivo*, we next investigated a potential role for *Penk1* in osteoblasts. Despite the absence of an overt bone phenotype *in vivo*, primary osteoblasts isolated from *Penk1*^{-/-} mouse calvariae showed an impairment of their metabolic and Alp activities, along with a lower nodule mineralization ability, compared to cells isolated from WT mice (**Figure 5 a-c**). Moreover, in a CFU-Fibroblastic assay, using bone marrow cells isolated from tibias, we observed a lower number and area of Alp-positive colonies in *Penk1*^{-/-} versus WT mice (**Figure 5d**), suggesting a cell autonomous positive effect of *Penk1* in osteoblasts.

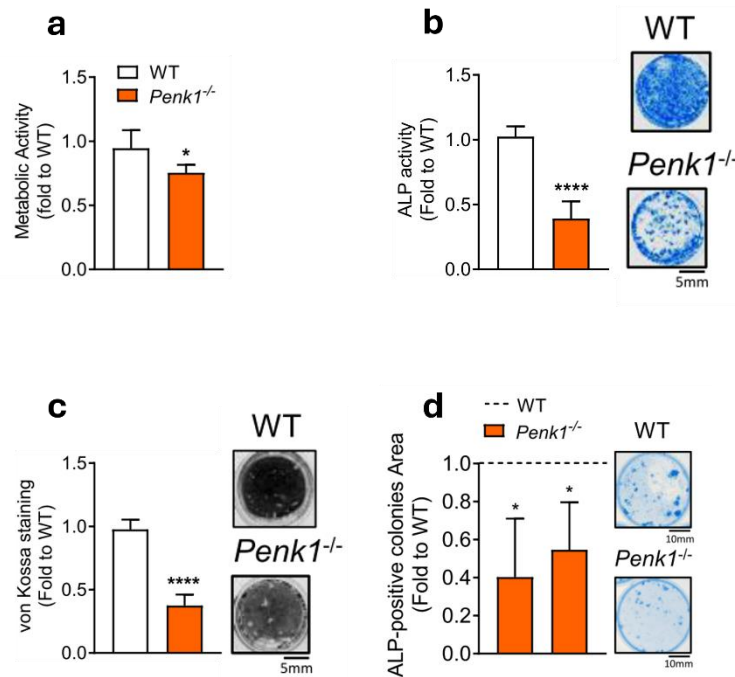


Figure 5: Effect of Penk 1 in osteoblast biology. Primary osteoblasts were isolated from the calvariae of 7-day-old WT and *Penk1*^{-/-} mice and evaluated for (a) cell metabolic activity assessed by the 3-(4,5-dimethylthiazol-2-yl)-2,5-diphenyltetrazolium (MTT) bromide reduction assay, (b) Alp activity by cytochemical assay and quantified by densitometric analysis (graph) and (c) von Kossa staining of mineralization nodules after 3 weeks of culture in osteogenic medium. (d) Osteogenic colony forming unit assay performed in bone marrow stromal cells flushed out from femurs of 7-day-old WT and *Penk1*^{-/-} mice. Data are the mean \pm SD of at least 3 mice or 3 cell preparations per group. * $p \leq 0.05$; ** $p = 0.0012$; *** $p \leq 0.001$; **** $p \leq 0.0001$ (Student's t test).

Next, we found that *Penk1* transcriptional expression increased during osteoblast differentiation in mouse primary osteoblasts cultured in osteogenic medium (Figure 6a). In line with this, *Penk1* mRNA downregulation in differentiated osteoblasts by treatment with specific *Penk1* siRNAs increased *Sclerostin* (*Sost*) while reducing *Wnt3a* and *Colla1* mRNAs, compared to cells treated with scrambled siRNA (SCR-siRNA, Figure 6b). In contrast, osteoblast differentiation markers, including *Akp2*, encoding for Alkaline phosphatase (*Alp*), *Runx2*, *Osterix* (*Osx*) and *Bone gamma-carboxyglutamic acid-containing protein* (*Bglap*) encoding for osteocalcin, were unremarkable (Figure 6b), indicating a possible role for *Penk1* in Wnt-mediated osteoblast anabolic activity rather than in osteoblast differentiation. In line with this observation, treatment of primary osteoblasts with Met-Enk, a *Penk1* product that activates the δ - and μ -opioid receptors, did not affect *Alp* activity (Figure 6c), while it increased nodule mineralization compared to vehicle-treated cells (Figure 6d). Consistently,

transcriptional analysis showed a significant increase of *Coll1a1* and *Osx* in Met-Enk-treated cells (Figure 6e).

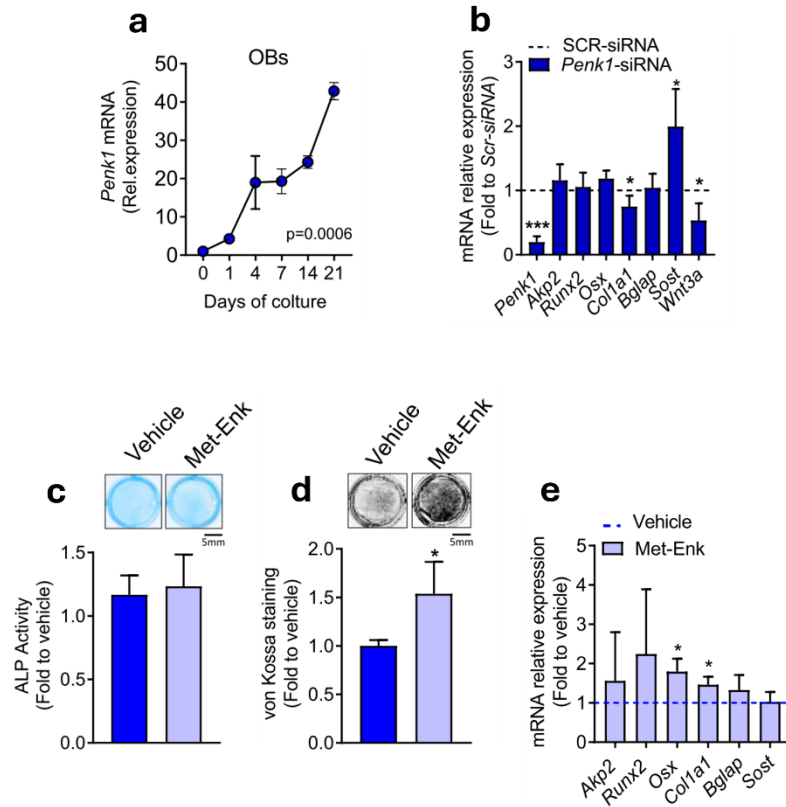


Figure 6: Effect of Penk 1 in osteoblast biology. (a) Time-course of *Penk1* mRNA expression in WT primary osteoblasts isolated from 7-day-old mice and cultured in standard medium supplemented with 10 mM β -glycerophosphate and 50 μ g/mL ascorbic acid (osteogenic medium). (b) Mouse primary osteoblasts were treated with scrambled (SCR) siRNA or with siRNAs specific for *Penk1* (Penk1-siRNA), after 48h the RNA was extracted, retro-transcribed in cDNA and subjected to real time RT-PCR for the indicated genes. Mouse primary osteoblasts were treated with vehicle or 1 μ M Met-Enkephalin (Met-Enk) for 48 hours. (c) Alp activity evaluated by histochemical assay and quantified by densitometric analysis (graph) and (d) vonKossa staining to evaluate nodule mineralization in osteoblasts treated with vehicle or 1 μ M Met-Enk for 2 weeks in the presence of osteogenic medium. (e) Transcriptional expression of the genes indicated in the abscissa, evaluated by real time RT-PCR, in Met-Enk-treated osteoblasts. Scale bars are indicated in the figures. Gene expression was normalized using mouse *Gapdh*. Data are the mean \pm SD of at least 3 mice or 3 cell preparations per group. **p* \leq 0.05; ****p* \leq 0.001. (Student's t test or in (a) RM-ANOVA).

Altogether this data demonstrated that Penk1 affects both osteoblast function and differentiation in a cell-autonomous manner, and that the transient deletion of *Penk1* in differentiated osteoblasts specifically impairs the osteoanabolic activity while its chronic deletion affects both differentiation and activity.

5. Discussion

Neuropeptides are involved in the regulation of bone metabolism, influencing the activity of bone cells, including osteoblasts, osteoclasts, and osteocytes^{31, 32, 103, 104}. Nevertheless, the role of opioids, a specific class of neuropeptides, in bone is still partially unclear and the complexity of their signaling pathways further complicates the scenario. Indeed, opioid receptors are known to be expressed in bone cells and opioid-derived peptides have been shown to have direct effects on bone metabolism^{31, 89, 104, 105}. When opioids bind to their receptors on bone cells, they can activate several signaling pathways that influence bone cell functions. As an example, the use of naltrexone and naloxone, two opioid growth factor receptor (OGFR) antagonists, stimulate bone formation *in vitro* and *vivo*^{106, 107}. Similar results were obtained in mice in which the expression of the opioid peptide dynorphin or its κ -opioid receptor were abolished¹⁰⁸. In contrast, D'Ângelo *et al.*¹⁰⁹ demonstrated that the blockade of the κ -opioid receptor increases osteoclast differentiation and bone resorption in rats. Seitz *et al.*⁹¹ observed a significant reduction of the osteoid formation in Phex-deficient Hyp mice in which *Penk1* expression was abolished *in vivo*, suggesting that *Penk1* is involved in the accumulation of non-mineralized bone matrix. A recent study showed that Met-Enk blocks osteocyte apoptosis by regulating the nuclear translocation of NFATc1 in the presence of compressive forces¹⁰³. Finally, different studies have shown that the chronic use of opioids can lead to decreased bone density and increased risk of fractures^{110, 111}.

It is therefore within this intricate context that our study is inserted, with the scope of understanding the role of *Penk1* in bone homeostasis under physiological conditions and in response to mechanical unloading. In line with our previous study, in which *Penk1* mRNA was downregulated in unloaded osteoblasts, in the present work we found that mechanical unloading leads to a reduction of *Penk1* expression both in mouse's and human's models of disuse osteoporosis. Moreover, we demonstrated an inverse correlation between *Penk1* serum levels and the time of unloading, suggesting that *Penk1* is highly responsive to this condition. These results not only suggest a possible role for *Penk1* in the response of the skeleton to unloading conditions but they also candidate *Penk1* as a possible marker of unloading-induced bone loss. Further study, including a larger cohort of human subjects, will be required to shed light on the underlining mechanisms. Indeed, the falls of *Penk1* level could be also involved in the onset of chronic bone pain afflicting people exposed to skeletal unloading condition, such as astronauts and bedridden people^{112, 113}.

Despite the data obtained in the microgravity experiments, no impact on bone phenotype was observed *in vivo* in *Penk1*^{-/-} mice, compared to wild type littermates. These findings are in line with the results reported by Seinz *et al.*⁹¹ on the lack of an overt bone phenotype in *Penk1*^{-/-} mice. They could be in part explained by the fact that residual circulating enkephalins are detectable in the sera of *Penk1*^{-/-} mice, as demonstrated by Seinz *et al.*⁹¹. A further explanation could be that the δ , κ and μ opioid receptors expressed by bone not only bind Penk1-derived enkephalins, but also other neuropeptides, such as β -endorphins and dynorphins, known to impact the bone metabolism^{89, 108, 107, 114}. Therefore, the combined effect of residual enkephalins and other neuropeptides on bone cells could potentially counterbalance the effect of the absence of *Penk1* *in vivo*. This conclusion was further supported by the presence of impaired differentiation and activity *in vitro* in osteoblasts isolated from *Penk1*^{-/-} mice, suggesting the presence of a cell-autonomous effect in these cells.

To further recognize the involvement of *Penk1* in bone metabolism, we investigated its role in osteoblast differentiation and activity. We found that *Penk1* is highly expressed in bone and in mature osteoblasts. In this regard, conflicting data are reported in the literature. Indeed Rosen *et al.*⁹⁵ demonstrated an inverse correlation between *Penk1* mRNA expression and osteoblast differentiation, while Seitz and colleagues⁹¹ found a higher expression of *Penk1* in differentiated cells. In our hands, *Penk1* is expressed by the bone tissue, in particular during osteoblast differentiation, and its suppression impacts on osteoblast differentiation and activity. Interestingly, we found that the transient deletion of *Penk1* in differentiated osteoblasts impairs specifically osteoanabolic activity but not differentiation, while its chronic germline deletion affects both differentiation and activity. These findings are in line with a possible dual role of osteoblastic Penk1 in embryos and adults, as postulated by Rosen and Bar-Shavit¹¹⁵. Moreover, in contrast with the observations of Nikhil *et al.*¹⁰⁷ we found that treatment of mature osteoblasts with Met-Enk increases nodule mineralization *in vitro*. To reconcile these results, we can speculate that probably Met-Enk increases nodule mineralization indirectly, by enhancing type I collagen expression and bone matrix deposition, without acting directly on mineral metabolism, as shown by our gene expression data and in part suggested by Seinz *et al.*⁹¹.

Mechanistically, we demonstrated that the Wnt pathway could be a potential candidate through which the Penk1 signalling acts on differentiated osteoblast activity. In fact, we showed that transient *Penk1* knock-down in differentiated osteoblasts increased the expression of the sclerostin encoding gene, *Sost1*, along with a parallel downregulation of *Wnt3a* and *Colla1*.

In conclusion, our work adds another piece of information to the intricate network of interactions between neuropeptides and skeletal tissues, confirming a role of *Penk1* in osteoblast differentiation and

activity and paving the way to future studies for dissecting the mechanisms underlining the involvement of Penk1 in unloading-induced bone loss.



Chapter 3: “Effect of Lipocalin-2 ablation on osteoblasts subjected to mechanical unloading.”

Manuscript in preparation

1. Abstract

Lipocalin-2 is a versatile molecule involved in different physiological and pathological processes. From previous works we know that this protein plays an important role in bone homeostasis and in osteoblasts response to mechanical unloading. Indeed, we found *Lcn2* to be the most upregulated gene in a whole gene profiling analysis performed in osteoblasts subjected to microgravity as a model of mechanical unloading. Moreover, simulated microgravity results in an impairment of osteoblast differentiation compared to unit gravity control condition. Therefore, to investigate whether genetic ablation of *Lcn2* can counteract the inhibitory effect of microgravity on osteoblast differentiation, we set up *in vitro* and *in vivo* experiments using mechanical unloading models. For the former, primary osteoblasts isolated from calvariae of WT and *Lcn2*^{-/-} mice were cultured at unit gravity (1g) or under modeled microgravity (0.008g) using the NASA-developed rotating wall vessel (RWV) bioreactor for 5 days. For the *in vivo* experiment, WT and *Lcn2*^{-/-} mice were subjected to Hindlimb suspension (HLS) by tail traction for 21 days. Our results demonstrated that, at least *in vitro*, *Lcn2* genetic ablation counteracts the reduction of *Runx2* and *Osx* transcriptional expression induced by microgravity. Moreover, *Lcn2* ablation also prevents the increase of Rankl/Opg ratio observed in the conditioned media of WT osteoblasts cultured under unloading conditions. However, in the mice subjected to HLS, the lack of *Lcn2* is not sufficient to counteract the bone loss due to mechanical unloading and disuse, although it is sufficient to prevent the number and the surface area of osteoblasts from decreasing, as observed to WT littermates subjected to HLS.

2. Introduction

Lipocalin-2 (LCN2), also known as Neutrophil Gelatinase-Associated Lipocalin (NGAL), is a glycoprotein of 22-25 kDa, purified for the first time by Kjeldsen *et al*³⁴ in 1993 from neutrophil granules released at sites of infection and inflammation. However, it is possible to refer to this protein also as adipokine, since it is highly produced by adipocytes¹¹⁶. Actually, LCN2 is expressed in a huge variety of cells, including hepatocytes, lung, bone marrow, macrophages, thymus, prostate, kidney and even in bone³⁵. As a member of the lipocalin superfamily, it transports small hydrophobic molecules such as steroids, fatty acids, retinoids, prostaglandins, and hormones¹¹⁷. In addition, LCN2 can bind iron, thus absolving also an antibacterial function and for this it is also known as siderocalin^{35, 117, 118}.

LCN2 is involved in several functions including innate immunity, inflammation, tumor progression and metastasis, acute kidney and liver injury, bone and muscle pathophysiology, cell differentiation, apoptosis, organogenesis, and even systemic insulin sensitivity, glucose homeostasis and lipid metabolism, although the exact role played in the last listed functions has not yet been fully described and is still unclear^{35, 96, 117, 118}.

Since 2009, our interest in LCN2 has been growing. In Capulli *et al.* (2009)⁷⁴ *Lcn2* has been identified as the most upregulated gene in primary murine osteoblasts maintained under simulated microgravity condition using the Rotating-wall vessel (RWV) bioreactor. Later on (Rucci *et al.*, 2015) our group demonstrated that *Lcn2* is a mechanoresponding gene able to regulate bone homeostasis; moreover, a direct correlation between LCN2 serum levels and the duration of the mechanical unloading in human subjects mimicked by HDTBR (Head Down Tilt Bed Rest) was found⁷¹. Similar results were obtained in the murine model of mechanical unloading, thus indicating a causative role for *Lcn2* in unloading induced bone loss. In addition, *Lcn2* overexpression in osteoblasts inhibit their differentiation, increase the expression of pro-osteoclastogenic factors *RankL* and *Il-6* and decrease the expression of *Opg*, an anti-osteoclastogenic factor, enhancing osteoblasts' ability to stimulate osteoclastogenesis⁷¹. Additional studies (Capulli *et al.*; 2018) proved that *Lcn2* has an important role in bone metabolism, in fact *Lcn2*^{-/-} mice display an osteopenic phenotype, characterized by a reduction of osteoblast number and activity, likely due to an alteration of the glucose metabolism observed in *Lcn2*^{-/-} mice³³. Finally, Ponzetti *et al.* (2022), found that the MDX mouse model of Duchenne Muscular Dystrophy (DMD), showed higher LCN2 serum levels compared to WT mice, while the ablation of *Lcn2* in these mice counteracted the bone loss due to the muscle failure and also ameliorate the muscle phenotype in MDX mice⁹⁶.

Based on this evidence we decided to investigate in deeper the role of LCN2 in osteoblasts homeostasis and whether the ablation of LCN2 could influence osteoblasts' response to unloading conditions.

3. Materials and methods

3.1 Materials

Dulbecco's modified Minimum Essential Medium (DMEM), penicillin, streptomycin, and trypsin were from Euroclone (Milan, Italy), Fetal Bovine Serum (FBS) was from GIBCO (Uxbridge, UK).

Sterile plastic ware was from Greiner bio-one (Kremsmünster, Austria) or Euroclone (Milan, Italy). TRIzol reagent (cat#15596018), primers and reagents for RT-PCR (cat#k1622) were from Invitrogen (Carlsbad, CA, USA). The qRT-PCR assays Luna Universal One-Step RT-qPCR Kit (#E3006) was from New England Biolab. LCN2(cat# MLCN20), RANKL (cat# MTR00) and OPG (cat#MOP00) ELISA assays were from R&D, Minneapolis, MN, USA, for interleukin (IL)6 ELISA kits (cat# ab100712) were from Abcam (Cambridge, UK) All other reagents were of the purest grade from Sigma Aldrich Co.(St. Louis, MO, USA).

3.2 Animals

Lcn2^{-/-} mice (background C57BL6/J, IMSR Cat# JAX:000664, RRID: IMSR_JAX:000664) were generated and kindly provided by Dr. Tak Wah Mak (University Health Network, Toronto, ON, Canada¹⁹). They are vital, with an overall normal lifespan and fertility. All procedures involving animals and their care were conducted in conformity with national and international laws and policies (European Economic Community Council Directive 86/609, OJ L 358, 1, December 12, 1987; Italian Legislative Decree 4.03.2014, n.26, Gazzetta Ufficiale della Repubblica Italiana no. 61, March 4, 2014) and animal procedures received approval by the Italian Ministry of Health authority (Approval N. 392/2020-PR). Mice were housed in the animal facility of the University of L'Aquila, Italy, at the following conditions: temperature: 20-24°C, humidity: 60%, dark/light cycle: 12/12 hours. They had access to food and water *ad libitum* and were fed with standard diet (Mucedola code: 4RF21).

3.3 Osteoblast primary cultures

Calvariae from 7-day-old WT and *Lcn2*^{-/-} mice were explanted, cleaned free of soft tissues, and digested three times with 1 mg/mL Clostridium histolyticum type IV collagenase and 0.25% trypsin, for 15, 30 and 45 min at 37°C, with gentle agitation. Cells from the second and third digestions were plated following centrifugation at 200g for 7 min and grown in DMEM plus 10% FBS. The purity of the culture was evaluated by the transcriptional expression of the osteoblast markers alkaline phosphatase (*Akp2*), Runt-related transcription factor 2 (*Runx2*), type I collagen, and osteocalcin and by the cytochemical evaluation of Alkaline phosphatase activity^{33, 119}.

At confluence, osteoblasts were trypsinized, collected and resuspended in DMEM 10% FBS containing CultiSpher-G1 microcarriers (1 g/L medium), at a cellular density of 1.2×10^6 cells/ml, to allow cell-microcarrier interaction. This suspension was then grown for 5 days into the RWV bioreactor under a 16-rpm rotation, which leads to a simulated microgravity condition of 0.008g, or in non-adhesive

Petri dishes, that is the unit gravity condition (1g)⁷⁴. At the end of the experiments, cells were collected and subjected to RNA extraction, while conditioned media (CM) were recovered for ELISA assays.

3.4 Comparative real-time RT-PCR

Total RNA was extracted Using the TRIzol ® method. 1µg of RNA was reverse transcribed into cDNA using Revert Aid First Strand cDNA Synthesis Kit (Invitrogen) and the equivalent of 0.1 µg was employed per PCR reaction using the Luna Universal One-Step RT-qPCR Kit (New England Biolab). Results, expressed as fold increase versus control, were normalized with the housekeeping gene glycerol-3-phosphate dehydrogenase (*Gapdh*). Primer sequences are reported in **Table 1** as follow:

Table 1 Real Time Primers sequences

Gene	Forward primer	Reverse primer
<i>Gapdh</i>	5'-TGTGAGGGAGATGCTCAGT-3'	5'-TGTTCTACCCCAATGTG-3'
<i>Lcn2</i>	5'-ACTGAATGGGTGGTG-3'	5'-GGGAGTGCTGGCCAA-3'
<i>Runx2</i>	5'-CCCAGCCACCTTTACCTACA-3'	5'-TATGGAGTGCTGCTGGTCTG-3'
<i>Osx</i>	5'-TGCTTCCCAATCCTATTTGC-3'	5'-AGAATCCCTTCCCTCTCCA-3'
<i>Akp2</i>	5'-CCAGCAGTTTCTCTCTTGG-3'	5'-CTGGGAGTCTCATCCTGAGC-3'
<i>Col1a1</i>	5'-CACCTCAAGAGCCTGAGTC-3'	5'-GTTCGGGCTGATGTACCAGT-3'
<i>Rankl</i>	5'-AGCCGAGACTACGGCAAGTA-3'	5'-CCACAATGTGTTGCAGTTCC-3'
<i>Opg</i>	5'-AGTCCGTGAAGCAGGAGTG-3'	5'-CCATCTGGACATTTTTTGCAA-3'
<i>Il-1β</i>	5'-GCCCATCCTCTGTGACTCAT-3'	5'-AGGCCACAGGTATTTTGTCG-3'
<i>Il-6</i>	5'-GTTCTCTGGAAATCGTGGA-3'	5'-GGAAATTGGGGTAGGAAGGA-3'

3.5 ELISA assay

Soluble Rankl, Opg and Lcn2 were quantified in the conditioned media using the R&D System ELISA kits cat# MLCN20, cat# MTR00, and cat#MOP00, respectively according to the manufacturer's instructions. The quantity of soluble Il-6 was evaluated in conditioned media using the Abcam ELISA kit #ab100712, following the protocol provided by the manufacturer.

3.6 Hindlimb suspension

Hindlimb suspension (HLS) was obtained according to Sakata and colleagues⁹⁴. Eight-week-old WT and *Lcn2*^{-/-} mice were suspended by tail traction using a strip of elastic tape and a swivel fixed to an

overhead wire, the height of which was adjusted to maintain the mice suspended at an approximately 30-degree angle. The swivel apparatus allowed animals ready access to food and water and to move freely into the cage using their forelimbs. After 21 days of suspension mice were euthanized by CO₂ inhalation, blood was harvested by intracardiac injection and sera were collected after coagulation and centrifugation. Hindlimbs were removed, cleaned from soft tissues and fixed in 4% buffered paraformaldehyde for histological analyses. An equal number of mice was maintained under normal cage conditions for 21 days as control.

3.7 MicroCT analysis

Femurs harvested from WT and *Lcn2*^{-/-} mice were fixed in 4% buffered paraformaldehyde and then images were acquired using the SkyScan 1174 (Bruker, Billerica, MA, USA) with a resolution of 6.7μm (X-ray voltage 50 kV). Image reconstruction was carried out employing a modified Feldkamp algorithm using the Skyscan Nrecon software. Three-dimensional (3D) and two-dimensional (2D) morphometric parameters were calculated for the trabecular bone, 150 slides (6.7μm thick) from the growth plate⁹⁶. 3D parameters were based on analysis of a Marching Cubes-type model with a rendered surface^{97, 98}. Calculation of all 2D areas and perimeters was based on the Pratt algorithm⁹⁹. Bone structural variables and nomenclature were those suggested by Bouxsein *et al.* (2010)¹⁰⁰. Cortical bone thickness was analyzed 450 slides below the growth plate on 100 slides as described¹⁰¹.

3.8 Bone histomorphometry

Tibiae harvested from WT and *Lcn2*^{-/-} mice were fixed in 4% buffered paraformaldehyde, dehydrated in ascending alcohol series, and processed for methyl–methacrylate embedding without decalcification. Osteoclast number/bone surface (Oc.N/BS) and osteoclast surface/bone surface (Oc.S/BS%) were evaluated after histochemical staining for TRAcP activity, while osteoblast number/bone surface (Ob.N/BS) and osteoblast surface/bone surface (Ob.S/BS%) were evaluated in sections stained with toluidine blue. Histomorphometric measurements were carried out on 5-μm-thick sections using the image analysis software NIH ImageJ and with the suggested nomenclature¹⁰². Dynamic assessment of the mineral apposition rate (MAR) was calculated after double injection of calcein, 10 and 3 days before euthanasia. Bone formation rate (BFR) was calculated according to the following formula: $MAR \times MS/BA$, where MS = mineralized surface and BA = bone area, as suggested by Dempster and colleagues¹⁰².

3.9 Statistics

Results are expressed as the mean \pm SD of at least 3 independent experiments, or at least 5 mice/group. Statistical analyses were performed by the Student's *t*-test, using the Graph pad Prism software (v8). A p-value <0.05 was considered statistically significant.

4. Results

4.1 Effect of *Lcn2* ablation on osteoblasts subjected to simulated microgravity

Results obtained from previous works^{33, 74, 71} identified *Lcn2* as a mechanoresponsive gene, which prompted us to investigate the effect of *Lcn2* ablation on the response of osteoblasts to mechanical unloading. For this purpose, osteoblasts isolated from calvariae of 7-day-old WT and *Lcn2*^{-/-} mice were cultured for 5 days under unit gravity (1g) or simulated microgravity conditions (0.008g) using the RWV bioreactor. First, we confirmed the upregulation of *Lcn2* in WT osteoblasts subjected to microgravity conditions, both transcriptionally (**Figure 1a**) and as protein released in the conditioned medium (**Figure 1b**).

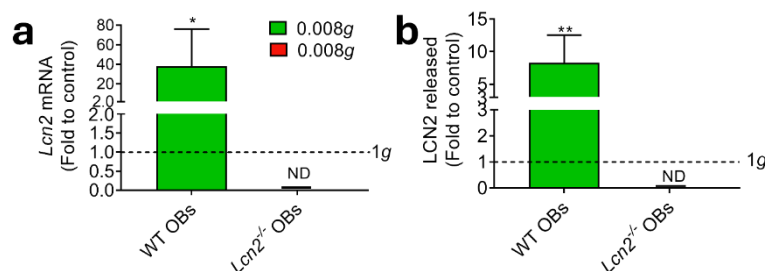


Figure 1: Lcn2 is overexpressed in osteoblasts under simulated microgravity. Primary osteoblasts isolated from the calvaria of 7-day-old WT (WT OBs) or *Lcn2*^{-/-} mice (*Lcn2*^{-/-} OBs) were cultured for 5 days under unit gravity (1g) or simulated microgravity (0.008 g) using the NASA approved Rotating Wall Vessel (RWV) bioreactor. **(a)** Transcriptional expression of *Lcn2* by real time RT-PCR. **(b)** ELISA assay performed on conditioned medium to quantify the secretion of Lcn2. Data are the mean \pm SD of 5 independent experiments (* $p=0.04$, ** $p=0.0023$ vs control set at 1, Student t-test, dotted line=unit gravity, 1g; ND= non detectable).

Interestingly, simulated microgravity induced in WT osteoblasts a reduction in *Runx2* (Runt-related transcription factor 2) and *Osx* (Osterix) transcriptional levels compared to control at 1g (**Figure 2a**), while this is not observed in *Lcn2*^{-/-} osteoblasts subjected to microgravity (**Figure 2b**). With regards to *Akp2* (Alkaline phosphatase) and *Coll1a1* (collagen type I alpha 1 chain) their transcriptional expression was not affected by microgravity in both genotypes (**Figure 2**). This data indicates that the lack of *Lcn2* counteracts the transcriptional downregulation of the master regulators of osteoblastogenesis *Runx2* and *Osx*.

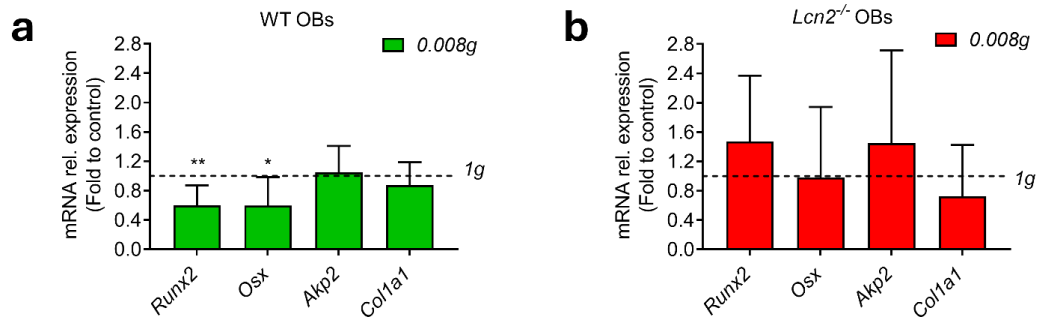


Figure 2: Effect of *Lcn2* ablation on osteoblasts response to simulated microgravity. Primary osteoblasts isolated from the calvaria of 7-day-old WT (WT OBs) or *Lcn2*^{-/-} mice (*Lcn2*^{-/-} OBs) were cultured for 5 days under unit gravity (1g) or simulated microgravity (0.008g) using the Rotating Wall Vessel (RWV) bioreactor. Evaluation of *Runx2* (Runt-related transcription factor 2), *Osx* (Osterix), *Akp2* (Alkaline phosphatase) and *Colla1* (Collagen type I a1) transcriptional levels in (a) WT and (b) *Lcn2*^{-/-} osteoblasts. Data are the mean \pm SD of 5 independent experiments (*p=0.028, **p=0.005 vs control set at 1, Student t-test; dotted line=unit gravity, 1g).

In agreement with Rucci *et al* (2007)¹²⁰, we observed a significant increase of *RankL* mRNA due to microgravity in WT osteoblasts (**Figure 3a**), while only a trend of increase in RankL was found in *Lcn2*^{-/-} osteoblasts under microgravity, which also had a much smaller magnitude of change vs control (**Figure 3b**). Moreover, *Opg* expression during microgravity conditions decreased in WT osteoblasts compared to the control (**Figure 3a**), while a trend of decrease was observed in *Lcn2*^{-/-} osteoblasts (**Figure 3b**). Interleukin -1 β and -6 transcriptional levels were not affected by simulated microgravity compared to control, neither in WT, nor in *Lcn2*^{-/-} osteoblasts (**Figure 3**). At protein level, in the culture media of WT osteoblasts subjected to 0.008g, the amount of secreted Rankl was higher than those quantified in the CM of the osteoblasts maintained at 1g (**Figure 3c**). For *Lcn2*^{-/-} osteoblasts, no significant difference in the amount of secreted Rankl can be appreciated between the samples cultured under microgravity conditions and at unit gravity (**Figure 3d**). We also evaluated the amount of secreted Opg in the CM. At variance with what observed at transcriptional level, ELISA assays showed a significant decrease of the secreted protein in the CM of the osteoblasts subjected to microgravity conditions compared to the control at 1g both for WT and *Lcn2*^{-/-} osteoblasts (**Figure 3c, 3d**). However, when we evaluated the Rankl/Opg ratio, this was significantly increased in WT osteoblasts subjected to microgravity, but not in *Lcn2*^{-/-} osteoblasts cultured at the same condition (**Figure 3e**). Moreover, we observed an increase of released IL-6 protein in the CM of the osteoblasts cultured at 0.008g compared to those maintained at 1g, in both WT and *Lcn2*^{-/-} cells (**Figure 3c, 3d**).

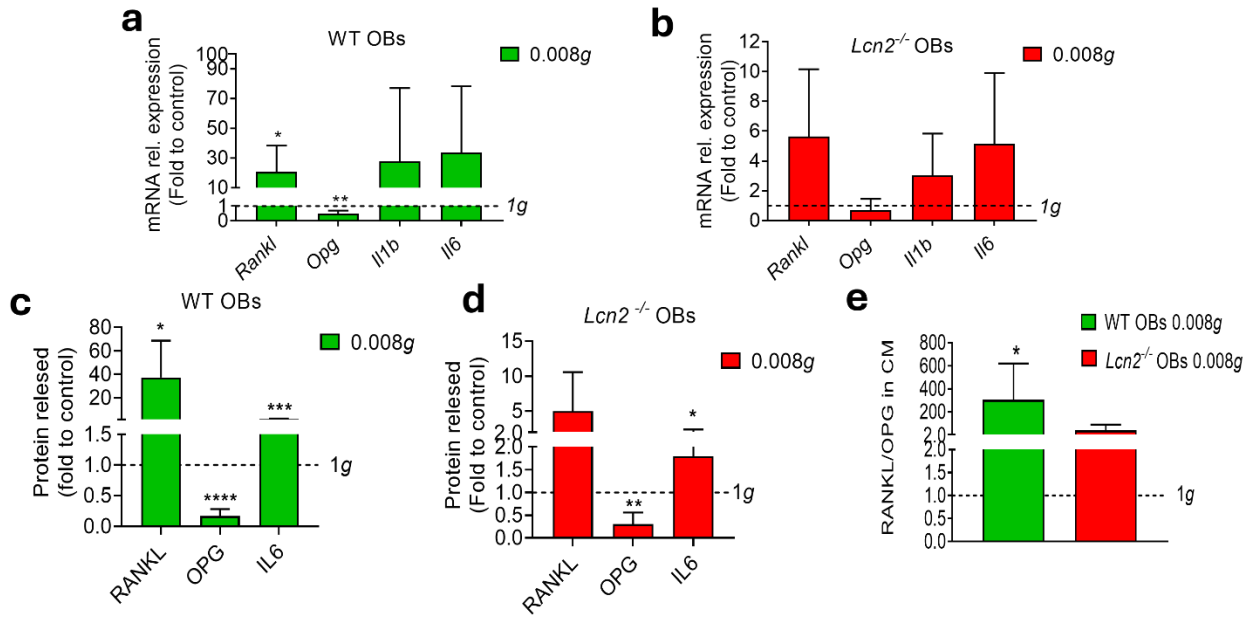


Figure 3: Effect of *Lcn2* ablation on osteoblasts response to simulated microgravity. Primary osteoblasts isolated from the calvaria of 7-day-old WT (WT OBs) or *Lcn2*^{-/-} mice (*Lcn2*^{-/-} OBs) were cultured for 5 days under unit gravity (1g) or simulated microgravity (0.008g) using the NASA approved Rotating Wall Vessel (RWV) bioreactor. (a,b) Transcriptional expression of the cytokines involved in osteoclastogenesis *Rankl*, *Opg*, *Il1b* and *Il6* in (a) WT and (b) *Lcn2*^{-/-} osteoblasts. (c,d) ELISA assay to assess (c) WT and (d) *Lcn2*^{-/-} osteoblast release of Rankl, Opg, Il6. (e) Evaluation of Rankl/Opg ratio. Data are the mean ± SD of 5 independent experiments (*p<0.05, **p<0.01, ***p<0.001, ****p<0.0001 vs control set at 1, Student t-test; dotted line=unit gravity, 1g)

Taken together, this data indicates that *Lcn2*, which is increased in osteoblasts subjected to microgravity likely promotes the decrease of *Runx2* and *Osx* and the increase of *RankL* mRNAs observed under the same conditions. Moreover, *Lcn2* promotes the increase of Rankl/Opg ratio observed in the CM of osteoblasts subjected to microgravity.

4.2 Effect of *Lcn2* ablation in the bones of mice subjected to mechanical unloading

In Capulli et al (2018)³³, our group demonstrated that *Lcn2*^{-/-} mice had a marked osteopenic phenotype due to reduced osteoblast number and activity, with no changes in osteoclast parameters. This phenotype was due to the impairment of the expression of Glut1 (glucose transporter 1) in the bone *Lcn2*^{-/-}, leading to energetically deregulated metabolism³³. Nevertheless, mechanical unloading resulted in bone loss as well as *Lcn2* increasing⁷¹.

To determine whether *Lcn2* ablation could abrogate the osteopenic effect of unloading in vivo, 8-week-old WT e *Lcn2*^{-/-} male mice were subjected to HLS for 3 weeks. WT and *Lcn2*^{-/-} male mice were also maintained in standard conditions (NLC=Normal Loading Condition) as control groups.

First, we confirmed the increase of *Lcn2* protein levels in serum of WT animals due to mechanical unloading, which is in agreement with our previous work⁷¹ (**Figure 4**).

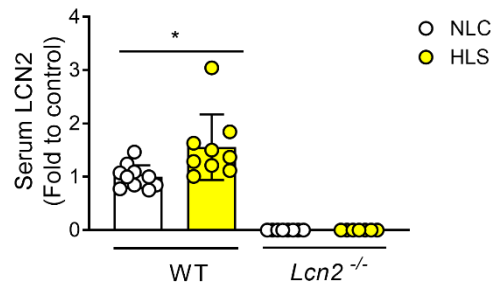


Figure 4: In vivo effect of unloading conditions on LCN2 serum levels in mice. Eight-week-old WT and *Lcn2*^{-/-} male mice were subjected to hindlimb suspension (HLS) for 3 weeks or maintained under normal loading conditions (NLC) as control groups. ELISA assay to assess LCN2 serum levels in mice subjected to mechanical unloading vs mice normal caged. (*p=0.01, Student t-test).

Micro-computed tomography (Micro-CT) analysis showed results in line with Du J *et al*¹²¹ and Rucci *et al*.⁷¹. In particular, in femur trabecular bone of WT mice HLS caused a reduction of bone volume/tissue volume (BV/TV%) and trabecular number (Tb.N.) as well as an increase of trabecular separation (Tb.Sp) and no modulation of trabecular thickness (Tb.Th.); moreover, mechanical unloading in the same mice decreased femurs' cortical thickness (Ct.Th.). Similar results were found for *Lcn2*^{-/-} mice subjected to mechanical unloading, excepting for trabecular separation which was not modulated. WT NLC mice show and higher Tb.N. and Tb Sp. compared to *Lcn2*^{-/-} NLC mice (**Figure 5**).

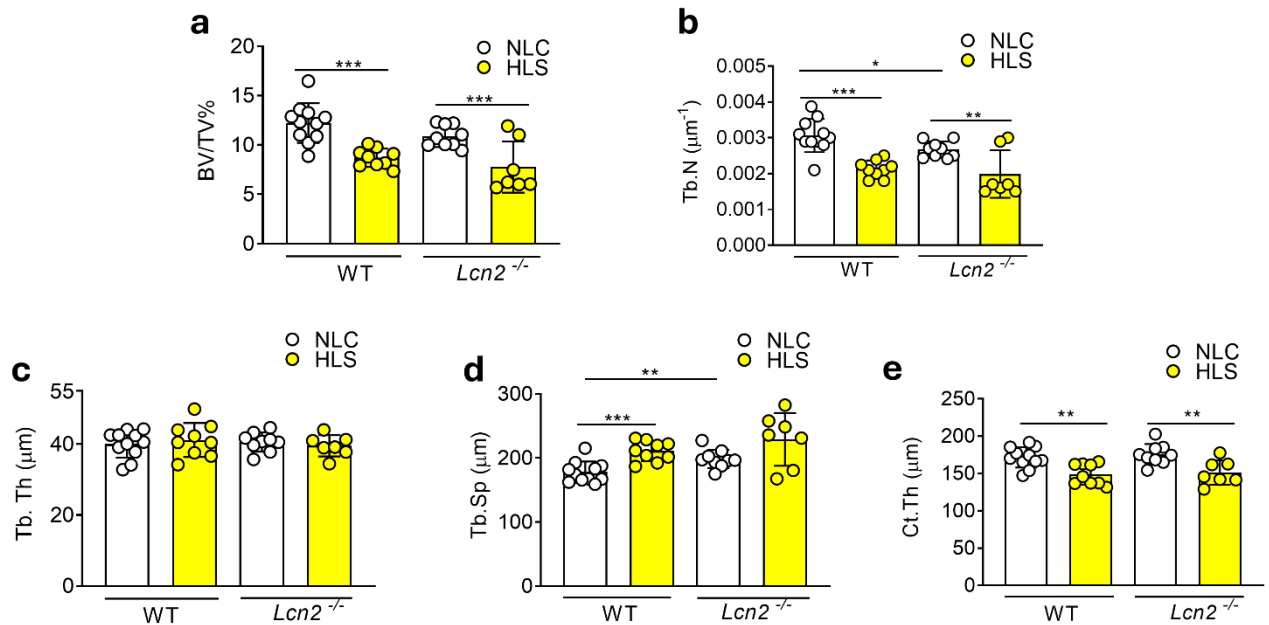


Figure 5: In vivo effect of *Lcn2* ablation on mechanical unloading-induced bone loss. Eight-week-old WT e *Lcn2*^{-/-} male mice were subjected to HLS for 3 weeks, in parallel, WT and *Lcn2*^{-/-} mice were maintained in NLC as control groups. Evaluation, by μ CT performed on explanted femurs, of (a) bone volume/tissue volume (BV/TV), (b) trabecular number (Tb.N), (c) trabecular thickness (Tb.Th), (d) trabecular separation (Tb.Sp), and (e) cortical thickness (Ct.Th), (* p <0.05, ** p <0.01, *** p <0.001, Student t-test).

Histomorphometric analysis revealed that in the tibiae of WT HLS mice the osteoclasts number over bone surface (Oc.N/BS) showed a trend towards increase compared to control ($p=0.07$), while no changes were observed in *Lcn2*^{-/-} mice bones (**Figure 6a**). osteoclasts surface over bone surface (Oc.S/BS) was not affected by mechanical unloading both in both genotype. (**Figure 6b**). As for osteoblasts, their number over bone surface (Ob.N/BS) was significantly reduced in the bone of WT mice subjected to unloading compared to WT NLC mice. Interestingly, in bone of *Lcn2*^{-/-} mice Ob.N/BS did not change between HLS and NLC (**Figure 6c**). Similar results were obtained for the osteoblasts surface over bone surface (Ob.S/BS), in fact, this parameter was lower in the tibiae of WT HLS mice than in WT NLC mice, while this decrease in unloading conditions was abrogate by *Lcn2* genetical ablation (**Figure 6d**). In order to evaluate the dynamic parameters bone formation rate (BFR) and mineral apposition rate (MAR), mice were subjected to a first injection of calcein ten days before takedown, and a second one, three days before takedown. Mechanical unloading reduced BFR in the bone of WT mice compared to control littermates but this detrimental effect of mechanical unloading was abrogated by the *Lcn2* ablation (**Figure 6e**).

Finally MAR was not affected by HLS both in WT and *Lcn2*^{-/-} mice (**Figure 6f**).

This result suggests that lack of *Lcn2* in the *in vivo* model of mechanical unloading prevents the reduction of osteoblast parameters and BFR in HLS mice, however this is not sufficient to prevent bone loss due to disuse.

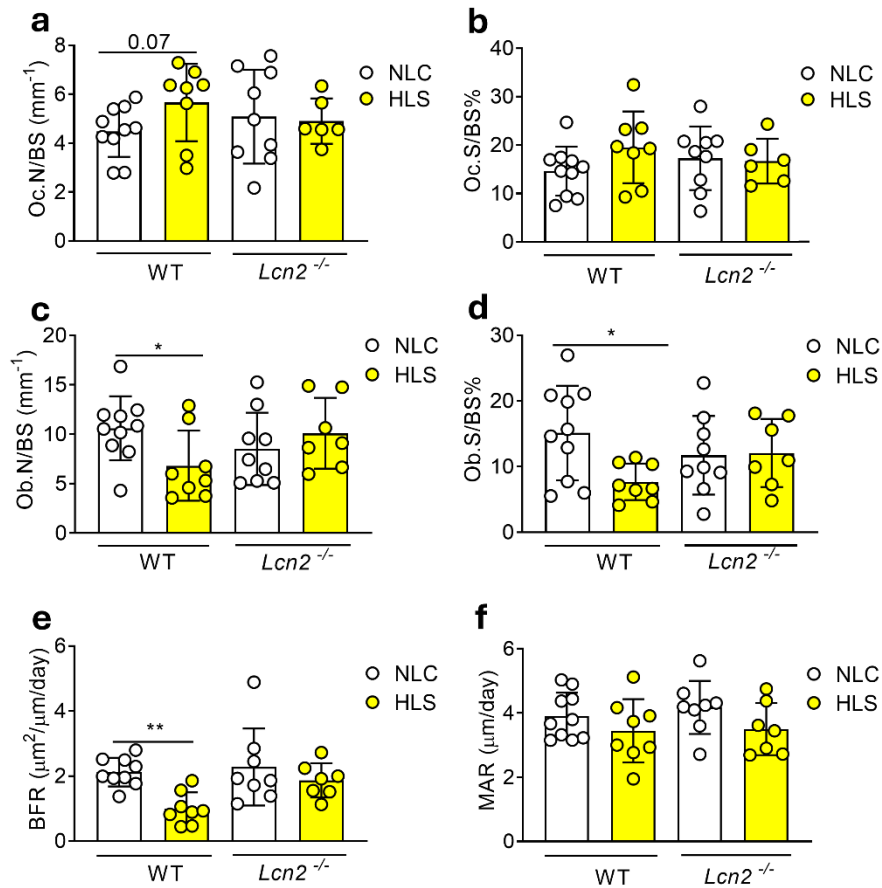


Figure 6: In vivo effect of *Lcn2* ablation on cellular bone parameters under mechanical unloading conditions. Eight-week-old WT e *Lcn2*^{-/-} male mice were subjected to HLS for 3 weeks, in parallel, WT and *Lcn2*^{-/-} mice were maintained in NLC as control groups. Histomorphometry performed on histological sections of tibiae, stained for (a,b) Tartrate-resistant acid phosphatase (TRAcP) activity to assess (a) osteoclast number per bone surface (Oc.N/BS) and (b) osteoclast surface per bone surface (Oc.S/BS%) and (c,d) stained with toluidine blue to evaluate (c) osteoblast number per bone surface (Ob.N/BS) and (d) osteoblast surface per bone surface (Ob.S/BS%). (e,f) Mice were subjected to a double injection (10 and 3 days prior sacrifice) of calcein In order to evaluate the following dynamic parameters: (e) Bone Formation Rate (BFR) and (f) Mineral Apposition Rate (MAR) (*p<0.05, **p=0.001, Student t-test).

5. Discussion

Several recent studies have shown Lipocalin-2 to partake in bone homeostasis^{50, 71, 122, 124, 125, 126} In our hands, this protein plays a key role in bone response to mechanical unloading^{96, 31, 71}. It is known that this phenomenon, which occurs during forced bed rest and long-duration space flight, is detrimental for bone, since the osteoblasts bone formation activity is inhibited, while osteoclasts resorptive activity could be enhanced, leading to disuse osteoporosis¹²⁶. Lipocalin 2 seems to be involved to the pathological response of the bone tissue to low mechanical forces, and in particular, it was found to be increased by simulated microgravity and unloading both *in vitro* and *in vivo*^{71, 74}.

The current study investigated whether the ablation of *Lcn2* could counteract the detrimental effect of unloading conditions on bone homeostasis. We found that simulated microgravity conditions, obtained by using the RWV bioreactor, reduced *Runx2*, *Osx* and *Opg* while increasing *RankL* expression levels in primary murine osteoblasts. Interestingly, the absence of *Lcn2* prevented these changes. In addition, accordingly with Rucci *et al* 2007¹²⁰, ELISA assays showed us that mechanical unloading prompted to the increase of Rankl/Opg ratio in the conditioned medium of WT osteoblasts compared to control maintained at 1g, whereas this increase does not occur for *Lcn2*^{-/-} osteoblasts. Given that Opg is a decoy receptor for Rankl¹²⁷, the lack of an increase in the Rankl/Opg ratio indicates that the ablation of *Lcn2* in osteoblasts may be able to counteract the pro-osteoclastogenic effect of microgravity demonstrated by Rucci *et al* in 2007¹²⁰.

Encouraged by *in vitro* results, we set up an *in vivo* mechanical unloading experiment, exploiting the HLS by tail traction on mice. Accordingly with previous results, the lack of *Lcn2* cancel the pro-osteoclastogenic effect of microgravity conditions, in fact, HLS induce no changes in osteoclasts parameters in tibiae of *Lcn2*^{-/-} mice, while in WT mice the mechanical unloading determine a trend of increase in Oc.N./BS. However, our results show that, although the absence of *Lcn2* is able to counteract the decrease of Ob.N/BS, Ob.S/BS%, and thus also the decrease in BFR, it is not sufficient to cancel out the bone loss due to mechanical unloading. Considering that ablation of *Lcn2* in MDX mouse model of Duchenne muscular dystrophy (DMD) counteracted the bone loss due to unloading/ disuse, the results obtained in this work may seem inconsistent with previous work⁹⁶. Nevertheless, in DMD are involved other factors that can be considered detrimental for bone in addition to disuse, such as inflammation and muscle damage, in which *Lcn2* is also known to be involved^{128, 129}.

In conclusion, our work shows that although this protein is definitely involved in the response of osteoblasts to mechanical unloading, genetic ablation of Lipocalin 2 is not sufficient to counteract bone loss due to mechanical unloading/disuse.



Chapter 4: “General discussion and conclusions”

1. General discussion and conclusions

In order to preserve its integrity and functionality, bone tissue is subjected to remodeling, consisting of a cycle of well programmed cellular events that lead to the resorption of old and damaged bone by osteoclasts, and deposition of new bone by osteoblasts ²². Bone remodeling is under the control of a very complex network of pathways, ensuring the perfect balance between osteoclasts and osteoblasts activity ^{8, 130}. Events which perturb osteoclasts and/or osteoblasts homeostasis, such as mechanical unloading, may result in the imbalance of this equilibrium, leading to pathological conditions, like disuse osteoporosis ⁴².

Starting from a previous work in which *Lcn2* and *Penk1* were identified, respectively, as the most up and downregulated genes in unloaded osteoblasts ⁷⁴, during my PhD I focused my research to evaluate the involvement of these molecules in osteoblasts homeostasis, particularly in response to mechanical unloading.

In **Chapter 2** of this thesis, we investigated the role of *Penk1* in bone under physiological conditions and in response to mechanical unloading. We confirmed *Penk1* downregulation in response to mechanical unloading in two animal models of disuse osteoporosis (HLS and Botox intramuscular injection). Moreover, we observed an inverse correlation between PENK1 protein levels and bed rest duration in sera of healthy volunteers subjected to bed rest. These results suggest a potential role for *Penk1* in osteoblasts' response to mechanical unloading.

Based on these premises we decided to evaluate physiological functions of *Penk1* in osteoblasts. We found that *Penk1* is expressed in mature osteoblasts and its gene expression progressively increased during osteoblasts differentiation *in vitro*. Overall, ablation of *Penk1* in mice did not affect bone phenotype *in vivo*, however transient silencing in mice osteoblasts impaired osteoblast activity, while the treatment of osteoblasts with Met-enkephalin, *Penk1* encoded peptide, improved osteoblasts activity. Finally, we evaluated the chronic deletion of *Penk1* in osteoblasts *in vitro*, observing that in *Penk1*^{-/-} osteoblasts both differentiation and activity were impaired. These controversial results may be explained by the fact that combined effect of residual enkephalins and other neuropeptides on bone cells could counterbalance the effect of the absence of *Penk1 in vivo* ^{89, 91, 108, 109, 114}. In fact, osteoblasts isolated from *Penk1*^{-/-} mice displayed impaired differentiation and activity, suggesting the presence of a cell-autonomous defect in these cells.

Future studies will be required to fully understand *Penk1* role in osteoblasts homeostasis and response to mechanical unloading, however our study added a piece of information to understand the mechanisms underlining the involvement of *Penk1* in unloading-induced bone loss.

In **Chapter 3** we dealt with *Lcn2*, this molecule was found to play an important role in osteoblasts' response to mechanical unloading, therefore we investigated whether the ablation of *Lcn2* could counteract bone loss due to unloading conditions. *In vitro* experiments showed that the lack of *Lcn2* prevented the reduction of *Runx2*, *Osx* and *Opg* and the increase of *RankL* expression levels in primary murine osteoblasts subjected to simulated microgravity using RWV bioreactor. In addition, as demonstrated by Rucci *et al* (2007)¹²⁰, mechanical unloading prompted to increase Rankl/Opg ratio in the conditioned medium of WT osteoblasts compared to control maintained at 1g, whereas the absence of *Lcn2* counteract this increase, indicating *Lcn2* ablation in osteoblasts may be able to prevent the pro-osteoclastogenic effect of microgravity demonstrated by Rucci *et al* in 2007¹²⁰.

In vitro results persuaded us to go deeper, evaluating the effect of *Lcn2* genetical ablation in hind limb suspension (HLS) mice, an animal model of mechanical unloading. Our results demonstrate that, absence of *Lcn2* is able to counteract the decrease of osteoblast number and surface observed in WT unloaded mice, as well as the decrease in BFR. However, this it is not sufficient to counteract the decrease of bone mass due to mechanical unloading.

In conclusion, although there is still a long way to go, the work done during my PhD adds another step forwards to understand the mechanisms of bone adaptation after mechanical unloading, demonstrating the role that *Penk1* and *Lcn2* play in this event, as well as the contribution of *Penk1* in osteoblast homeostasis. It is also important to point out that these studies not only allow to understand the mechanisms underlying bone loss during long-duration space flight, but they are also exploitable and applicable to those pathological circumstances in which patients experience disuse induced-bone loss as a consequence of paralysis or neuromuscular disorders. Our studies, although more comprehensive investigations will be required, provide evidence that serum levels of LCN2 and PENK1 may be useful markers of disuse bone loss and suggest that blocking LCN2 and/or increasing Met-Enkephalin levels could represent viable therapeutic options for disuse osteoporosis.

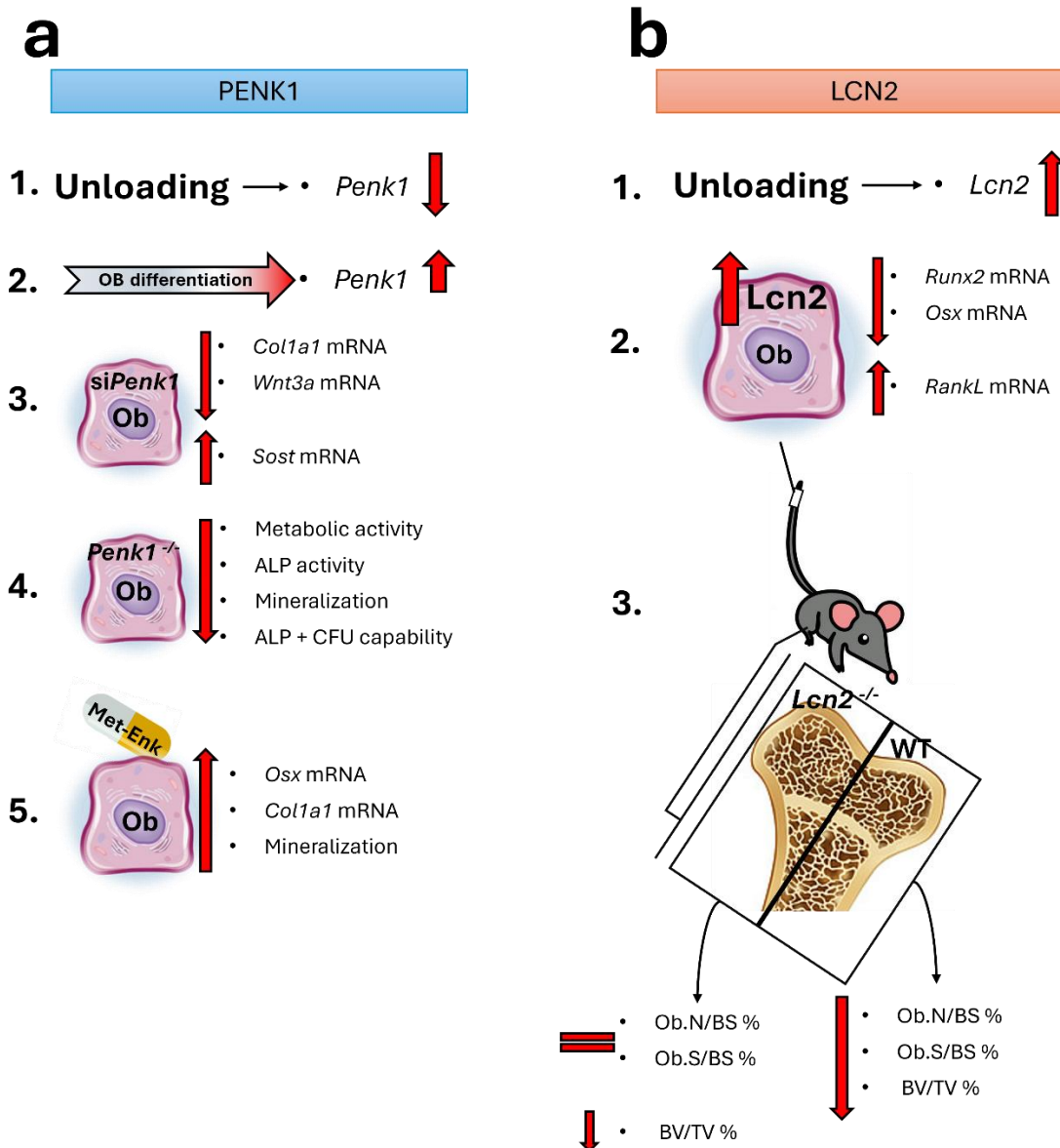


Figure 1: Graphical abstract of the main findings of the thesis. This thesis examined the role of *Penk1* (a) and *Lcn2* (b) in bone homeostasis under physiological conditions and in response to mechanical unloading. Mechanical unloading leads to a reduction of *Penk1* expression both in mouse and human models of disuse osteoporosis (a.1.). *Penk1* is highly expressed in osteoblasts, in particular during differentiation (a.2.). The transient downregulation of *Penk1* in differentiated osteoblasts impairs specifically osteoanabolic activity but not their differentiation (a.3.), while its chronic germline deletion affects both differentiation and activity (a.4.). Treatment of mature osteoblasts with Met-Enk increases nodule mineralization in vitro (a.5.). *Lcn2* was found to be increased by simulated microgravity and unloading both in *vitro* and in *vivo* (b.1.). *Lcn2* is involved in the pathological response of the bone tissue to low mechanical forces, and in particular in the reduction of *Runx2* and *Osx* relative expression, along with the increase of *RankL* transcriptional levels due to unloading (b.2.). In *vivo* results showed that the absence of *Lcn2* is able to counteract the decrease of Ob.N/BS%, Ob.S/BS%, and thus also the decrease in BFR, although it is not sufficient to cancel out the bone loss due to mechanical unloading (b.3.). **Ob**= osteoblast.



Chapter 5: “References”

References

1. Florencio-Silva R., Sasso G. R., Sasso-Cerri E. Simões, M. J., Cerri, P. S. *Biology of Bone Tissue: Structure, Function, and Factors That Influence Bone Cells*. BioMed research international, 2015; 2015: 421746. doi: 10.1155/2015/421746
2. Hart N. H., Newton R. U., Tan J., Rantalainen T., Chivers P., Siafarikas A., Nimphius S. *Biological basis of bone strength: anatomy, physiology and measurement*. Journal of musculoskeletal & neuronal interactions, 2020; 20(3), 347–371.
3. Adamo S., De Felici M., Dolfi A., Filippini A., Grano M., Musarò A., Nervi C., Papaccio G., Salustri A., Ziparo E., Bernardini N., Boitani C., Bonsi L., M. Bouchè, Brun P., Canipari R., Castriconi R., Castrogiovanni P., Ciccarelli C., De Cesaris P., M. De, D. V. *Istologia di Monesi*. (2018)
4. Nather A., Ong H. J. C., Aziz Z. *Structure of Bone. Bone Grafts and Bone Substitutes: Basic Science and Clinical Applications*, 3-17 (2005).
5. Šromová V, Sobola D, Kaspar P. *A Brief Review of Bone Cell Function and Importance*. Cells. 2023;12(21):2576. doi:10.3390/cells12212576.
6. Lin X, Patil S, Gao YG, Qian A. *The Bone Extracellular Matrix in Bone Formation and Regeneration*. Front Pharmacol. 2020;11:757. doi:10.3389/fphar.2020.00757
7. Alford AI, Kozloff KM, Hankenson KD. *Extracellular matrix networks in bone remodeling*. Int J Biochem Cell Biol. 2015;65:20-31. doi:10.1016/j.biocel.2015.05.008
8. Bolamperti S, Villa I, Rubinacci A. *Bone remodeling: an operational process ensuring survival and bone mechanical competence*. Bone Res. 2022;10(1):48. doi:10.1038/s41413-022-00219-8.
9. Del Fattore A, Teti A, Rucci N. *Bone cells and the mechanisms of bone remodeling*. Front Biosci (Elite Ed). 2012;4(6):2302-2321. doi:10.2741/543
10. Teti A. *Bone development: overview of bone cells and signaling*. Curr Osteoporos Rep. 2011;9(4):264-273. doi:10.1007/s11914-011-0078-8

11. Capulli M, Paone R, Rucci N. *Osteoblast and osteocyte: games without frontiers*. Arch Biochem Biophys. 2014;561:3-12. doi:10.1016/j.abb.2014.05.003
12. Fetter AW, Switzer WP, Capen CC. *Electron microscopic evaluation of bone cells in pigs with experimentally induced Bordetella rhinitis (turbinate osteoporosis)*. Am J Vet Res. 1975;36(1):15-22.
13. Cappariello A, Maurizi A, Veeriah V, Teti A. *The Great Beauty of the osteoclast*. Arch Biochem Biophys. 2014;558:70-78. doi:10.1016/j.abb.2014.06.017
14. Robling, Alexander G. and Bonewald, Lynda F. *The Osteocyte: New Insights* Annual Review of Physiology 2020; 82: 485-506. doi: 10.1146/annurev-physiol-021119-034332
15. McDonald M. M., Kim A. S., Mulholland B. S., Rauner M. *New Insights Into Osteoclast Biology*. JBMR plus, 2021; 5(9), e10539. doi:10.1002/jbm4.10539
16. Kodama J., Kaito T. *Osteoclast Multinucleation: Review of Current Literature*. International journal of molecular sciences, 2020; 21(16), 5685. <https://doi.org/10.3390/ijms21165685>
17. Maurizi A, Rucci N. *The Osteoclast in Bone Metastasis: Player and Target*. Cancers (Basel). 2018;10(7):218. doi:10.3390/cancers10070218
18. Feng X, Teitelbaum SL. *Osteoclasts: New Insights*. Bone Res. 2013;1(1):11-26. doi:10.4248/BR201301003
19. Adamopoulos IE, Mellins ED. *Alternative pathways of osteoclastogenesis in inflammatory arthritis*. Nat Rev Rheumatol. 2015;11(3):189-194. doi:10.1038/nrrheum.2014.198
20. Lorenzo J. *The many ways of osteoclast activation*. The Journal of clinical investigation, 2017; 127(7), 2530–2532. <https://doi.org/10.1172/JCI94606>
21. Frost HM. *Bone Remodeling Dynamics*. Springfield, IL: Thomas, 1963.
22. Kenkre JS, Bassett J. *The bone remodeling cycle*. Ann Clin Biochem. 2018;55(3):308-327. doi:10.1177/0004563218759371
23. Hadjidakis DJ, Androulakis II. *Bone remodeling*. Ann N Y Acad Sci. 2006;1092:385-396. doi:10.1196/annals.1365.035

24. Owen R, Reilly GC. *In vitro Models of Bone Remodeling and Associated Disorders*. Front Bioeng Biotechnol. 2018;6:134. doi:10.3389/fbioe.2018.00134
25. Ponzetti M., Aielli F., Ucci A., Cappariello A., Lombardi G., Teti A., Rucci, N *Lipocalin 2 increases after high-intensity exercise in humans and influences muscle gene expression and differentiation in mice*. J Cell Physiol. 2022;237(1):551-565. doi:10.1002/jcp.30501
26. Cappariello A, Muraca M, Teti A, Rucci N. *Circulating Extracellular Vesicles Express Receptor Activator of Nuclear Factor κ B Ligand and Other Molecules Informative of the Bone Metabolic Status of Mouse Models of Experimentally Induced Osteoporosis*. Calcif Tissue Int. 2023;112(1):74-91. doi:10.1007/s00223-022-01032-5
27. Konttinen Y.T., Imai S., Suda A., *Neuropeptides and the puzzle of bone remodeling: State of the art*, Acta Orthopaedica Scandinavica 1996; 67(6) 632-639.
28. Marie PJ. *Fibroblast growth factor signaling controlling bone formation: an update*. Gene. 2012;498(1):1-4. doi:10.1016/j.gene.2012.01.086
29. Yavropoulou MP, Yovos JG. *The role of the Wnt signaling pathway in osteoblast commitment and differentiation*. Hormones (Athens). 2007;6(4):279-294. doi:10.14310/horm.2002.1111024
30. Ducy P, Zhang R, Geoffroy V, Ridall AL, Karsenty G. *Osf2/Cbfa1: a transcriptional activator of osteoblast differentiation*. Cell. 1997;89(5):747-754. doi:10.1016/s0092-8674(00)80257-3
31. Comb M, Seeburg PH, Adelman J, Eiden L, Herbert E. *Primary structure of the human Met- and Leu-enkephalin precursor and its mRNA*. Nature. 1982;295(5851):663-666. doi:10.1038/295663a0
32. Fricker L.D., Margolis E.B., Gomes I., Devi L.A., *Five Decades of Research on Opioid Peptides: Current Knowledge and Unanswered Questions*, Molecular Pharmacology 2020;98(2) 96-108 doi: 10.1124/mol.120.119388
33. Capulli M, Ponzetti M, Maurizi A, Gemini-Piperni S, Berger T, Mak TW, Teti A, Rucci N. *A Complex Role for Lipocalin 2 in Bone Metabolism: Global Ablation in Mice Induces Osteopenia Caused by an Altered Energy Metabolism*. J Bone Miner Res. 2018;33(6):1141-1153. doi:10.1002/jbmr.3406

34. Kjeldsen L, Johnsen AH, Sengeløv H, Borregaard N. *Isolation and primary structure of NGAL, a novel protein associated with human neutrophil gelatinase*. J Biol Chem. 1993;268(14):10425-10432
35. Jaber SA, Cohen A, D'Souza C, Abdulrazzaq YM, Ojha S, Bastaki S, Adeghate EA. *Lipocalin-2: Structure, function, distribution and role in metabolic disorders*. Biomed Pharmacother. 2021;142:112002. doi:10.1016/j.biopha.2021.112002
36. Rauner M., Taipaleenmäki H., Tsourdi E., Winter E. M. *Osteoporosis Treatment with Anti-Sclerostin Antibodies-Mechanisms of Action and Clinical Application*. Journal of clinical medicine, 2021;10(4), 787. doi:10.3390/jcm10040787
37. Choi JUA, Kijas AW, Lauko J, Rowan AE. *The Mechanosensory Role of Osteocytes and Implications for Bone Health and Disease States*. Front Cell Dev Biol. 2022;9:770143. doi:10.3389/fcell.2021.770143
38. Qin L., Liu W., Cao H., Xiao G. *Molecular mechanosensors in osteocytes*. Bone research, 2020; 8, 23. doi:10.1038/s41413-020-0099-y
39. Rose D, Preethi T., KC Arul Prakasam A *Review on Osteoporosis*. JARESM, 2022; 2455-6211.
40. Eastell R, O'Neill TW, Hofbauer LC, Langdahl B, Reid IR, Gold DT, Cummings SR. *Postmenopausal osteoporosis*. Nat Rev Dis Primers. 2016;2:16069. doi:10.1038/nrdp.2016.69.
41. Hangartner TN. *Osteoporosis Due to Disuse*, Physical Medicine and Rehabilitation Clinics of North America, 1995;6(3)579-594, doi: 10.1016/S1047-9651(18)30457-1.
42. Rolvien T, Amling M. *Disuse Osteoporosis: Clinical and Mechanistic Insights*. Calcif Tissue Int. 2022;110(5):592-604. doi:10.1007/s00223-021-00836-1
43. Alexandre C, Vico L. *Pathophysiology of bone loss in disuse osteoporosis*. Joint Bone Spine. 2011;78(6):572-576. doi:10.1016/j.jbspin.2011.04.007
44. Abdelrahman S, Ireland A, Winter EM, Purcell M, Coupaud S. *Osteoporosis after spinal cord injury: aetiology, effects and therapeutic approaches*. J Musculoskelet Neuronal Interact. 2021;21(1):26-50.

45. Iolascon, G., Paoletta, M., Liguori, S., Curci, C., Moretti, A. *Neuromuscular Diseases and Bone*. *Frontiers in endocrinology* 2019; 10, 794. doi: 10.3389/fendo.2019.00794
46. Jiang SD, Jiang LS, Dai LY. *Mechanisms of osteoporosis in spinal cord injury*. *Clin Endocrinol (Oxf)*. 2006;65(5):555-565. doi:10.1111/j.1365-2265.2006.02683.x
47. Dionyssiotis Y, Kalke YB, Frotzler A, Moosburger J, Trovas G, Kaskani E, Erhan B, Foti C, Papathanasiou J, Ferretti JL, Imamura M, Rapidi AC; HeSCOSPRM Bone and Spinal Cord Injury Working Group Attendants. *SI Guidelines on Bone Impairment in Spinal Cord Injury*. *J Clin Densitom*. 2021;24(3):490-501. doi:10.1016/j.jocd.2021.03.009
48. Varacallo M, Davis DD, Pizzutillo P. *Osteoporosis in Spinal Cord Injuries*. *StatPearls* [Internet]. Treasure Island (FL): 2024; PMID: 30252365.
49. Lau, R. Y., & Guo, X. *A review on current osteoporosis research: with special focus on disuse bone loss*. *Journal of osteoporosis*, 2011;293808. doi.10.4061/2011/293808
50. Man J, Graham T, Squires-Donnelly G, Laslett AL. *The effects of microgravity on bone structure and function*. *NPJ Microgravity*. 2022;8(1):9. doi:10.1038/s41526-022-00194-8
51. Tilton FE, Degioanni JJ, Schneider VS. *Long-term follow-up of Skylab bone demineralization*. *Aviat Space Environ Med*. 1980;51(11):1209-1213.
52. Caillot-Augusseau A, Lafage-Proust MH, Soler C, Pernod J, Dubois F, Alexandre C. *Bone formation and resorption biological markers in cosmonauts during and after a 180-day space flight (Euromir 95)*. *Clin Chem*. 1998;44(3):578-585.
53. Sibonga JD, Evans HJ, Sung HG, Spector E.R, Lang T.F, Oganov V.S, Bakulin A.V, Shackelford L.C, LeBlanc A.D. *Recovery of spaceflight-induced bone loss: bone mineral density after long-duration missions as fitted with an exponential function*. *Bone*. 2007;41(6):973-978. doi:10.1016/j.bone.2007.08.022
54. Stavnichuk M, Mikolajewicz N, Corlett T, Morris M, Komarova SV. *A systematic review and meta-analysis of bone loss in space travelers*. *NPJ Microgravity*. 2020;6:13. doi:10.1038/s41526-020-0103-2

55. Nabavi N, Khandani A, Camirand A, Harrison RE. *Effects of microgravity on osteoclast bone resorption and osteoblast cytoskeletal organization and adhesion*. *Bone*. 2011;49(5):965-974. doi:10.1016/j.bone.2011.07.036
56. Blaber EA, Dvorochkin N, Lee C, Alwood JS, Yousuf R, Pianetta P, Globus RK, Burns BP, Almeida EA. *Microgravity induces pelvic bone loss through osteoclastic activity, osteocytic osteolysis, and osteoblastic cell cycle inhibition by CDKN1a/p21*. *PLoS One*. 2013;8(4):e61372. doi:10.1371/journal.pone.0061372
57. Pandiarajan M., Hargens A. R. *Ground-Based Analogs for Human Spaceflight*. *Frontiers in physiology*, 2020;11, 716. doi: 10.3389/fphys.2020.00716
58. Madaro, L., Smeriglio, P., Molinaro, M., & Bouché, M. *Unilateral immobilization : a simple model of limb atrophy in mice*. *Basic Applied Myology* 2008;18 (5): 149-153,
59. Brent, M. B., Lodberg, A., Thomsen, J. S., Brüel, A. *Rodent model of disuse-induced bone loss by hind limb injection with botulinum toxin A*. *MethodsX*, 2020; 7, 101079. doi. 10.1016/j.mex.2020.101079
60. Morey-Holton ER, Globus RK. *Hindlimb unloading rodent model: technical aspects*. *J Appl Physiol*. 2002;92(4):1367-1377. doi:10.1152/jappphysiol.00969.2001
61. Peurière L, Mastrandrea C, Vanden-Bossche A. *Hindlimb unloading in C57BL/6J mice induces bone loss at thermoneutrality without change in osteocyte and lacuno-canalicular network*. *Bone*.2023;169:116640. doi:10.1016/j.bone.2022.116640
62. Nishimura Y. *Technology using simulated microgravity*. *Regen Ther*. 2023;24:318-323. doi:10.1016/j.reth.2023.08.001
63. Jack J.W.A. van Loon, *Some history and use of the random positioning machine, RPM, in gravity related research*, *Advances in Space Research*, 2007;39(7) 1161:1165 doi:10.1016/j.asr.2007.02.016.
64. Tu X, Joeng KS, Nakayama KI, Nakayama K, Rajagopal J, Carroll TJ, McMahon AP, Long F. *Noncanonical Wnt signaling through G protein-linked PKCdelta activation promotes bone formation*. *Dev Cell*. 2007;12(1):113-127. doi:10.1016/j.devcel.2006.11.003

65. Chang J, Sonoyama W, Wang Z, Jin Q, Zhang C, Krebsbach PH, Giannobile W, Shi S, Wang CY. Noncanonical Wnt-4 signaling enhances bone regeneration of mesenchymal stem cells in craniofacial defects through activation of p38 MAPK. *Noncanonical Wnt-4 signaling enhances bone regeneration of mesenchymal stem cells in craniofacial defects through activation of p38 MAPK*. J Biol Chem. 2007;282(42):30938-30948. doi:10.1074/jbc.M702391200
66. Schena F, Menale C, Caci E, Diomedede L, Palagano E, Recordati C, Sandri M, Tampieri A, Bortolomai I, Capo V, Pastorino C, Bertoni A, Gattorno M, Martini A, Villa A, Traggiai E, Sobacchi C. *Murine Rankl^{-/-} Mesenchymal Stromal Cells Display an Osteogenic Differentiation Defect Improved by a RANKL-Expressing Lentiviral Vector*. Stem Cells. 2017;35(5):1365-1377. doi:10.1002/stem.2574
67. Kebuchi Y, Aoki S, Honma M, Hayashi M, Sugamori Y, Khan M, Kariya Y, Kato G, Tabata Y, Penninger JM, Udagawa N, Aoki K, Suzuki H. *Coupling of bone resorption and formation by RANKL reverse signalling*. Nature. 2018;561(7722):195-200. doi:10.1038/s41586-018-0482-7
68. Navasiolava NM, Custaud MA, Tomilovskaya ES, Larina IM, Mano T, Gauquelin-Koch G, Gharib C, Kozlovskaya IB. *Long-term dry immersion: review and prospects*. Eur J Appl Physiol. 2011;111(7):1235-1260. doi:10.1007/s00421-010-1750-x
69. Lang SM, Kazi AA, Hong-Brown L, Lang CH. *Delayed recovery of skeletal muscle mass following hindlimb immobilization in mTOR heterozygous mice*. PLoS One. 2012;7(6):e38910. doi:10.1371/journal.pone.0038910
70. Warner S. E., Sanford D. A., Becker B. A., Bain S. D., Srinivasan S., Gross T. S. *Botox induced muscle paralysis rapidly degrades bone*. Bone, 2006;38(2), 257–264. doi:10.1016/j.bone.2005.08.009
71. Rucci N, Capulli M, Piperni SG, Cappariello A, Lau P, Frings-Meuthen P, Heer M, Teti A. *Lipocalin 2: a new mechanoresponding gene regulating bone homeostasis*. J Bone Miner Res. 2015 Feb;30(2):357-68. doi: 10.1002/jbmr.2341. PMID: 25112732.
72. Rucci N, Migliaccio S, Zani BM, Taranta A, Teti A. *Characterization of the osteoblast-like cell phenotype under microgravity conditions in the NASA-approved Rotating Wall Vessel bioreactor (RWV)*. J Cell Biochem. 2002;85(1):167-179.

73. Hu H, Hilton MJ, Tu X, Yu K, Ornitz DM, Long F. *Sequential roles of Hedgehog and Wnt signaling in osteoblast development*. Development. 2005;132(1):49-60. doi:10.1242/dev.01564
74. Capulli M, Rufo A, Teti A, Rucci N. *Global transcriptome analysis in mouse calvarial osteoblasts highlights sets of genes regulated by modeled microgravity and identifies a "mechanoresponsive osteoblast gene signature"*. J Cell Biochem. 2009;107(2):240-252. doi:10.1002/jcb.22120
75. Cappariello A, Ponzetti M, Rucci N. *The "soft" side of the bone: unveiling its endocrine functions*. Horm Mol Biol Clin Investig. 2016;28(1):5-20. doi:10.1515/hmbci-2016-0009
76. Wang X, Xu J, Kang Q. *Neuromodulation of bone: Role of different peptides and their interactions* (Review). Mol Med Rep. 2021;23(1):32. doi:10.3892/mmr.2020.11670
77. Kontinen Y, Imai S, Suda A. *Neuropeptides and the puzzle of bone remodeling*. State of the art. Acta Orthop Scand. 1996;67(6):632-639. doi:10.3109/17453679608997772
78. Lutz PE, Kieffer BL. *Opioid receptors: distinct roles in mood disorders*. Trends Neurosci. 2013;36(3):195-206. doi:10.1016/j.tins.2012.11.002.
79. R. Przewłocki, B. Przewłocka, *Opioids in chronic pain*, Eur J Pharmacol 429(1-3) (2001) 79-91.
80. Barron B.A., *Opioid peptides and the heart*, Cardiovasc Res, England, 1999, pp. 13-6.
81. Janković B.D., Radulović J., *Enkephalins, brain and immunity: modulation of immune responses by methionine-enkephalin injected into the cerebral cavity*, Int J Neurosci 67(1-4) (1992) 241-70.
82. Holzer P., *Opioid receptors in the gastrointestinal tract*, Regul Pept 155(1-3) (2009) 11-7.
83. Keshet E., Polakiewicz R.D., Itin A., Ornoy A., Rosen H., *Proenkephalin A is expressed in mesodermal lineages during organogenesis*, Embo j 8(10) (1989) 2917-23.
84. Kew D., Kilpatrick D.L., *Widespread organ expression of the rat proenkephalin gene during early postnatal development*, Mol Endocrinol 4(2) (1990) 337-40.
85. Barron B.A., Oakford L.X., Gaugl J.F., Caffrey J.L., *Methionine-enkephalin-Arg-Phe immunoreactivity in heart tissue*, Peptides 16(7) (1995) 1221-7.

86. Denning G.M., Ackermann L.W., Barna T.J., Armstrong J.G., Stoll L.L., N.L. Weintraub, Dickson E.W., *Proenkephalin expression and enkephalin release are widely observed in non-neuronal tissues*, *Peptides* 29(1) (2008) 83-92.
87. Rosen H., Polakiewicz R.D., Benzakine S., Bar-Shavit Z., *Proenkephalin A in bone-derived cells*, *Proc Natl Acad Sci U S A* 88(9) (1991) 3705-9.
88. Elhassan, J.U. Lindgren A.M., Hultenby K., Bergstrom J., Adem A., *Methionine-enkephalin in bone and joint tissues*, *J Bone Miner Res* 13(1) (1998) 88-95.
89. Rosen H., Krichevsky A., Bar-Shavit Z., *The enkephalinergic osteoblast*, *J Bone Miner Res* 13(10) (1998) 1515-20.
90. Rosen H., Krichevsky A., Polakiewicz R.D., Benzakine S., Bar-Shavit Z., *Developmental regulation of proenkephalin gene expression in osteoblasts*, *Mol Endocrinol* 9(11) (1995) 1621-31.
91. Seitz S., Barvencik F., Gebauer M., Albers J., Schulze J., Streichert T., Amling M., Schinke T., *Preproenkephalin (Penk) is expressed in differentiated osteoblasts, and its deletion in Hyp mice partially rescues their bone mineralization defect*, *Calcif Tissue Int* 86(4) (2010) 282-93.
92. König M., Zimmer A.M., Steiner H., Holmes P.V., Crawley J.N., Brownstein M.J., Zimmer A., *Pain responses, anxiety and aggression in mice deficient in pre-proenkephalin*, *Nature* 383(6600) (1996) 535-538
93. Pérez-Castrillón L., Olmos J.M., Gómez J.J., Barrallo A., Riancho J.A, Perera L., Valero C., Amado J.A., González-Macías J., *Expression of opioid receptors in osteoblast-like MG-63 cells, and effects of different opioid agonists on alkaline phosphatase and osteocalcin secretion by these cells*, *Neuroendocrinology* 72(3) (2000) 187-94.
94. Sakata T., Sakai A., Tsurukami H., Okimoto N., Okazaki Y, Ikeda S., Norimura T., Nakamura T., *Trabecular bone turnover and bone marrow cell development in tail-suspended mice*, *J Bone Miner Res* 14(9) (1999) 1596-604.
95. Frings-Meuthen P., Buehlmeier J., Baecker N., Stehle P., Fimmers R., May F., Kluge G., Heer M., *High sodium chloride intake exacerbates immobilization-induced bone resorption and protein losses*, *J Appl Physiol* (1985) 111(2) (2011) 537-42.

96. Ponzetti M., Ucci A., Maurizi A., Giacchi L., Teti A., Rucci N., *Lipocalin 2 Influences Bone and Muscle Phenotype in the MDX Mouse Model of Duchenne Muscular Dystrophy*, *Int J Mol Sci* 23(2) (2022).
97. Lorensen W.E., Cline H.E., *Marching cubes: A high resolution 3D surface construction algorithm*, *ACM SIGGRAPH Computer Graphics* 21(4) (1987) 163-169.
98. Feldkamp L.A., Davis L.C., Kress J.W., *Practical cone-beam algorithm*, *Journal of the Optical Society of America A* 1(6) (1984) 612-619.
99. Pratt W., *Digital image processing*, 2nd ed., Wiley, New York, 1991.
100. Bouxsein M.L., Boyd S.K., Christiansen B.A., Guldberg R.E., Jepsen K.J., Müller R., *Guidelines for assessment of bone microstructure in rodents using micro-computed tomography*, *J Bone Miner Res* 25(7) (2010) 1468-86.
101. Rufo A., Del Fattore A., Capulli M., Carvello F., De Pasquale L., Ferrari S., Pierroz D., Morandi L., De Simone M., Rucci N., Bertini E., Bianchi M.L., De Benedetti F., Teti A., *Mechanisms inducing low bone density in Duchenne muscular dystrophy in mice and humans*, *J Bone Miner Res* 26(8) (2011) 1891-903.
102. Dempster D.W., Compston J.E., Drezner M.K., Glorieux F.H., Kanis J.A., Malluche H., Meunier P.J., Ott S.M., Recker R.R., Parfitt A.M., *Standardized nomenclature, symbols, and units for bone histomorphometry: a 2012 update of the report of the ASBMR Histomorphometry Nomenclature Committee*, *J Bone Miner Res* 28(1) (2013) 2-17.
103. Sogi C., Takeshita N., Jiang W., Kim S., Maeda T., Yoshida M., Oyanagi T., Ito A., Kimura S., Seki D., Takano I., Sakai Y., Fujiwara I., Kure S., Takano-Yamamoto T., *Methionine Enkephalin Suppresses Osteocyte Apoptosis Induced by Compressive Force through Regulation of Nuclear Translocation of NFATc1*, *JBMR Plus* 4(7) (2020) e10369.
104. Chen Q.C., Zhang Y., *The Role of NPY in the Regulation of Bone Metabolism*, *Front Endocrinol (Lausanne)* 13 (2022) 833485.

105. Janas A., Folwarczna J., *Opioid receptor agonists may favorably affect bone mechanical properties in rats with estrogen deficiency-induced osteoporosis*, *Naunyn Schmiedebergs Arch Pharmacol* 390(2) (2017) 175-185.
106. Tanaka K., Kondo H., Hamamura K, Togari A., *Systemic administration of low-dose naltrexone increases bone mass due to blockade of opioid growth factor receptor signaling in mice osteoblasts*, *Life Sci* 224 (2019) 232-240.
107. Thakur N.A., DeBoyace S.D., Margulies B.S., *Antagonism of the Met5-enkephalin-opioid growth factor receptor-signaling axis promotes MSC to differentiate into osteoblasts*, *J Orthop Res* 34(7) (2016) 1195-205.
108. Baldock P.A., Driessler F., Lin S., Wong I.P., Shi Y, Yulyaningsih E., Castillo L., Janmaat S., Enriquez R.F, Zengin A., Kieffer B.L., Schwarzer C., Eisman J.A, Sainsbury A., Herzog H., *The endogenous opioid dynorphin is required for normal bone homeostasis in mice*, *Neuropeptides* 46(6) (2012) 383-94.
109. D'Ângelo Q. M, Queiroz-Junior, C.M. Maltos, K.L.M. Ferreira, A.J. Pacheco, Soares C. R.V., *The blockade of kappa opioid receptors exacerbates alveolar bone resorption in rats*, *Arch Oral Biol* 120 (2020) 104923
110. Yue,Q. Ma Y., Teng Y., Zhu Y., Liu H., Xu S., Liu J., Zhang X., Teng Z., *An updated analysis of opioids increasing the risk of fractures*, *PLoS One* 15(4) (2020) e0220216.
111. Coluzzi F., Pergolizzi J., Raffa R.B., Mattia C., *The unsolved case of "bone-impairing analgesics": the endocrine effects of opioids on bone metabolism*, *Ther Clin Risk Manag* 11 (2015) 515-23.
112. Mantyh P.W., *The neurobiology of skeletal pain*, *Eur J Neurosci* 39(3) (2014) 508-19.
113. Penchev R., Scheuring R.A., Soto A.T., Miletich D.M., Kerstman E., Cohen S.P., *Back Pain in Outer Space*, *Anesthesiology* 135(3) (2021) 384-395.
114. Maldonado R., Baños J.E., Cabañero D., *Usefulness of knockout mice to clarify the role of the opioid system in chronic pain*, *Br J Pharmacol* 175(14) (2018) 2791-2808.

115. Rosen H., Bar-Shavit Z., *Dual role of osteoblastic proenkephalin derived peptides in skeletal tissues*, J Cell Biochem 55(3) (1994) 334-9.
116. Zhang Y, Foncea R, Deis JA, Guo H, Bernlohr DA, Chen X. *Lipocalin 2 expression and secretion is highly regulated by metabolic stress, cytokines, and nutrients in adipocytes*. PLoS One. 2014;9(5):e96997. doi:10.1371/journal.pone.0096997
117. Flower D. R. *The lipocalin protein family: structure and function*. The Biochemical journal, 318 (Pt 1)(Pt 1), 1–14. doi: 10.1042/bj3180001
118. Lögdberg L, Wester L. *Immunocalins: a lipocalin subfamily that modulates immune and inflammatory responses*. Biochim Biophys Acta. 2000;1482(1-2):284-297. doi:10.1016/s0167-4838(00)00164-3
119. Marzia, M., Sims, N. A., Voit, S., Migliaccio, S., Taranta, A., Bernardini, S., Faraggiana, T., Yoneda, T., Mundy, G. R., Boyce, B. F., Baron, R., & Teti, A. *Decreased c-Src expression enhances osteoblast differentiation and bone formation*. The Journal of cell biology, 2000;151(2), 311–320 doi: /10.1083/jcb.151.2.311
120. Rucci N, Rufo A, Alamanou M, Teti A. *Modeled microgravity stimulates osteoclastogenesis and bone resorption by increasing osteoblast RANKL/OPG ratio*. J Cell Biochem. 2007;100(2):464-473. doi:10.1002/jcb.21059
121. Du J, Yang J, He Z, Cui J, Yang Y, Xu M, Qu X, Zhao N, Yan M, Li H, Yu Z. *Osteoblast and Osteoclast Activity Affect Bone Remodeling Upon Regulation by Mechanical Loading-Induced Leukemia Inhibitory Factor Expression in Osteocytes*. Front Mol Biosci. 2020;7:585056. doi:10.3389/fmolb.2020.585056
122. Mosialou I, Shikhel S, Liu JM, Maurizi A, Luo N, He Z, Huang Y, Zong H, Friedman RA, Barasch J, Lanzano P, Deng L, Leibel RL, Rubin M, Nickolas T, Chung W, Zeltser LM, Williams KW, Pessin JE, Kousteni S. *MC4R-dependent suppression of appetite by bone-derived lipocalin 2* [published correction appears in Nature. 2017 Jun 14;546(7658):440]. Nature. 2017;543(7645):385-390. doi:10.1038/nature21697

123. Lim WH, Wong G, Lim EM, Byrnes E, Zhu K, Devine A, Pavlos NJ, Prince RL, Lewis JR. *Circulating Lipocalin 2 Levels Predict Fracture-Related Hospitalizations in Elderly Women: A Prospective Cohort Study*. J Bone Miner Res. 2015;30(11):2078-2085. doi:10.1002/jbmr.2546
124. Maurizi A, Ponzetti M, Gautvik KM, Reppe S, Teti A, Rucci N. *Lipocalin 2 serum levels correlate with age and bone turnover biomarkers in healthy subjects but not in postmenopausal osteoporotic women*. Bone Rep. 2021;14:101059. doi:10.1016/j.bonr.2021.101059
125. Costa D, Lazzarini E, Canciani B, Giuliani A, Spanò R, Marozzi K, Manescu A, Cancedda R, Tavella S. *Altered bone development and turnover in transgenic mice over-expressing lipocalin-2 in bone*. J Cell Physiol. 2013;228(11):2210-2221. doi:10.1002/jcp.24391
126. Loid P, Hauta-Alus H, Mäkitie O, Magnusson P, Mäkitie RE. *Lipocalin-2 is associated with FGF23 in WNT1 and PLS3 osteoporosis*. Front Endocrinol (Lausanne). 2022;13:954730. doi:10.3389/fendo.2022.954730
127. Lacey DL, Timms E, Tan HL, Kelley MJ, Dunstan CR, Burgess T, Elliott R, Colombero A, Elliott G, Scully S, Hsu H, Sullivan J, Hawkins N, Davy E, Capparelli C, Eli A, Qian YX, Kaufman S, Sarosi I, Shalhoub V, Senaldi G, Guo J, Delaney J, Boyle WJ. *Osteoprotegerin ligand is a cytokine that regulates osteoclast differentiation and activation*. Cell. 1998;93(2):165-176. doi:10.1016/s0092-8674(00)81569-x
128. An HS, Yoo JW, Jeong JH, Heo M, Hwang SH, Jang HM, Jeong EA, Lee J, Shin HJ, Kim KE, Shin MC, Roh GS. *Lipocalin-2 promotes acute lung inflammation and oxidative stress by enhancing macrophage iron accumulation*. Int J Biol Sci. 2023;19(4):1163-1177. doi:10.7150/ijbs.79915
129. Asaf S, Maqsood F, Jalil J, Sarfraz Z, Sarfraz A, Mustafa S, Ojeda IC. *Lipocalin 2-not only a biomarker: a study of current literature and systematic findings of ongoing clinical trials*. Immunol Res. 2023;71(3):287-313. doi:10.1007/s12026-022-09352-2



Chapter 6: “Achievements”

Curriculum Vitae et Studiorum



Chiara Puri

Born in Rieti (Italy),

19th June 1991,

Italian Citizenship



OrcidID QR code

ADDRESS

Via Dei Piccolomini, 8

67100, L'Aquila (AQ)

Italy

PHONE AND EMAIL

HOME → +39 08621760136

MOBILE → +39 3899322935

chiara.puri@ univaq.it

purichiara@gmail.com

ACADEMIC DEGREES

04/2019 Master's Degree in Pharmaceutical Biotechnologies *cum laude*. University of Perugia, Italy.

10/2016 Bachelor's degree in Biotechnologies. University of L'Aquila, Italy.

PROFESSIONAL EXPERIENCES

02/2023-to date Research Assistant (assegnista di ricerca) in the University of L'Aquila, Italy, in the "Skeletal Disease laboratory" headed by Prof. Nadia Rucci.

11/2020-10/2023 PhD candidate in Experimental Medicine (with scholarship, XXXVI cycle) in the University of L'Aquila, Italy, in the "Skeletal Diseases Lab" (Prof. Nadia Rucci)

02-11/2020 Research fellow in the "Skeletal Diseases Lab" (Prof. Nadia Rucci)

07/2018-04/2019 Student training in the "Photochemistry Lab" supervised by Prof. Catia Clementi

OTHER EXPERIENCES AND INITIATIVES

2021-2023 Volunteering: member and chair of the “Student Group” in the Thursday Morning Science (TMS) group, University of L’Aquila, Italy.

PUBLICATIONS:

- **Puri, C.**; Pucciarini, L.; Tiecco, M.; Brighenti, V.; Volpi, C.; Gargaro, M.; Germani, R.; Pellati, F.; Sardella, R.; Clementi, C. Use of a Zwitterionic Surfactant to Improve the Biofunctional Properties of Wool Dyed with an Onion (*Allium cepa* L.) Skin Extract. *Antioxidants* 2020, 9, 1055. doi: 10.3390/antiox9111055

- Ponzetti M, Ucci A, **Puri C**, Giacchi L, Flati I, Capece D, Zazzeroni F, Cappariello A, Rucci N and Falone S (2022) Effects of osteoblast-derived extracellular vesicles on aggressiveness, redox status and mitochondrial bioenergetics of MNNG/HOS osteosarcoma cells. *Front. Oncol.* 12:983254. doi: 10.3389/fonc.2022.983254

- **Puri, C.**, Dannenberg, C., Ucci, A., Ponzetti, M., Pucci, E., Silvestri, L., Lau, P., Frings-Meuthen, P., Heer, M., Rucci, N., Teti, A., Maurizi, A. (2024). Pre-proenkephalin 1 is Downregulated Under Unloading and is Involved in Osteoblast Biology. *Calcified tissue international*, 114(5), 524–534. doi: 10.1007/s00223-024-01199-z.

Date of preparation

May 2024

Chiara Puri

